EASI-STRESS

EUROPEAN ACTIVITY FOR STANDARDIZATION OF INDUSTRIAL RESIDUAL STRESS CHARACTERIZATION

H2020 NMBP-35-2020

Grant Agreement Number: 953219

Deliverable Report:

D3.2 Report on SOPs for instruments dedicated to bulk analysis and to near-surface analysis

Project Deliverable Information Sheet

EASI-STRESS Project	Project Ref. No. 953219	
	Project Title: EASI-STRESS - European Activity for Standardization of Industrial residual STRESS characterization	
	Project Website: www.easi-stress.eu	
	Deliverable No.: D3.2	
	Deliverable Type: Report	
	Dissemination Level: Public	Contractual Delivery Date: 31/12/2022
		Actual Delivery Date: 22/01/2023
	EC Project Officer: Yanaris Ortega Garcia	

Document Control Sheet

Document	Title: Report on SOPs for instruments dedicated to bulk analysis and to near-surface analysis	
	Version: 1.0	
	Available at: EASI-STRESS project TEAMS site	
	Files: EASI-STRESS_D3.2_FINAL.pdf	
Authorship	Written by	Mohamed Fares Slim/ESRF
	Contributors	David Canelo-Yubero/Hereon Sandra Cabeza/ILL Arnold Paecklar/ILL Thilo Pirling/ILL Thomas Buslaps/ESRF Peter Staron/Hereon Andrea Francesco Ciuffini/ESRF Guilherme Abreu Faria/Hereon Márton Markó/EK Gyula Török/EK
	Reviewed by	Ennio Tito Capria/ESRF Hanna Leemreize/DTI
	Approved	Nikolaj Zangenberg/DTI

List of Figures

List of Tables

List of Abbreviations

0D	0-Dimension
1D	1-Dimension
2D	2-Dimension
3D	3-Dimension
ADXRD	Angle Dispersive X-Ray Diffraction
BNC	Budapest Neutron Centre
CCD	Charge-Coupled Device
CRL	Compound Refractive Lens
CSC	Conical Slit Cell
DOI	Digital Object Identifier
DSP	Digital Signal Processor
EDXRD	Energy-Dispersive X-Ray Diffraction
EDM	Electrical Discharge Machining
EH	Experimental Hutch
FEM	Finite Element Modelling
FDS	Fonden Dansk Standard
FWHM	Full Width at Half Maximum
GV	Gauge Volume
HEMS	High Energy Materials Science
HW	Hardware
ID	Insertion Device
LRI	Large-scale Research Infrastructure
MCA	Multi-Channel Analyser
ND	Neutron Diffraction
NIPS	Neutron Induced Prompt gamma Spectrometer
PGAA	Prompt Gamma Activation Analyser
PSD	Position-Sensitive Detector
SOP	Standard Operating Procedure
SW	Software
TAS	Three Axis Spectrometer
TOF	Time Of Flight
TS	Technical Specification
UAG	User Advisory Group

Table of Contents

Executive Summary

Developing a basis for standardization of the determination of residual stresses by industries through Large-scale Research Infrastructures (LRI), guidelines, Technical Specifications (TS), and Standard Operating Procedures (SOPs) have been established for calibrations and measurements, alignment, validation, and data acquisition.

First, a brief introduction about diffraction and continuum mechanics of residual stresses has been reported, to better understand the context. Also, an overview of each experimental methodology has been detailed and datasheets, to be consulted by the User Advisory Group (UAG), are delivered in this report. The main guidelines, TS and SOPs have been reported for each experimental technique. Finally, the experimental procedures and the operative guidelines have been described.

The purpose of this report is to provide the current best operating procedures LRIs and the needed material to be consulted by the UAG.

Report on SOPs for instruments dedicated to bulk analysis and to near-surface analysis

1.   Introduction

Multiple developments, tailored to suit the needs of industry at LRIs both photon (X-ray) and neutron sources, have been made in the last decades. The design and application of many unique material systems have been greatly ameliorated by the knowledge achieved through the access at LRIs of industrial players (Petry, 2015) (Suzuki, 2014).

Actual metallic materials processing and forming techniques generate a state of internal strain. High-energy X-ray and neutron sources at LRIs offer unique opportunities to obtain a strain mapping in relatively thick samples and with good spatial resolution, non-destructively. This would allow finer computational processing models validations, stress-relief processes measurements, fitness for service ratifications, deeper failure analysis investigations, and, finally, much more accurate prototype or product validations.

Although the use of LRIs by industries leads to glaring, consistent, and long-lasting benefits, both the high-value and high-volume manufacturing sectors industries still run up against obstacles to accessing these facilities (Felcher, 1989). Part of these perceived barriers are linked to a low rationalization, standardization, and reliability of the measurement process, in terms of stability and repeatability, and also a low throughput. To lower and break down these perceived barriers is one of the main aims of EASI-STRESS. To achieve this goal, this report introduces a common framework and shared specifications: a reference sample system has been developed and adopted by LRIs, calibrations and measurements have been rationalized through established guidelines, alignment & validation and data acquisition have been standardized through the definition of Technical Specifications (TS) and Standard Operating Procedures (SOPs). The form of feedback and assessment practice will be exploited, granting a continuous improvement of the system. Moreover, brief guidelines and datasheets to be consulted by the User Advisory Group (UAG) are delivered in this report.

Further standardization actions will be studied and may be developed and implemented within WP6, together with an internal certification of the instruments in collaboration with Fonden Dansk Standard (FDS).

2.   Generalities

Diffraction techniques are the most exploited measures to achieve a non-destructive quantification of residual stresses. These measures are based on the physical principle described by the Bragg's diffraction law, interacting with a crystal lattice deformed by the residual stress field. These strains are the measured quantity to determine the residual stresses, comparing the diffraction peak to those measured on an unloaded/stress-free reference lattice and measuring their shifts. In the following, a

brief description of physical principles, continuum mechanics, and their interactions exploited in diffraction residual stresses measurements are addressed.

2.1. Bragg's Law

A penetrating neutron or X-ray beam, which illuminates a polycrystalline material with wavelengths similar to the interplanar spacings and fulfilling Bragg's condition, is diffracted producing distinct Bragg peaks. The relation between the lattice spacing d^{hkl} of the lattice planes determined by three integer Miller indices h, k, l, the diffraction angle 2θ and the wavelength λ or the energy E of the incident X-ray or neutron beam is defined by the Bragg's law (Eq. 1, Eq. 2, Fig. 1):

$$d^{hkl} = \frac{\lambda}{2 \times \sin \theta^{hkl}}$$

Eq. 1

or:

$$d^{hkl} = \frac{hc}{2 \times \sin \theta \times E^{hkl}}$$

Eq. 2

Where h is the Planck's constant and c the velocity of light in vacuum.
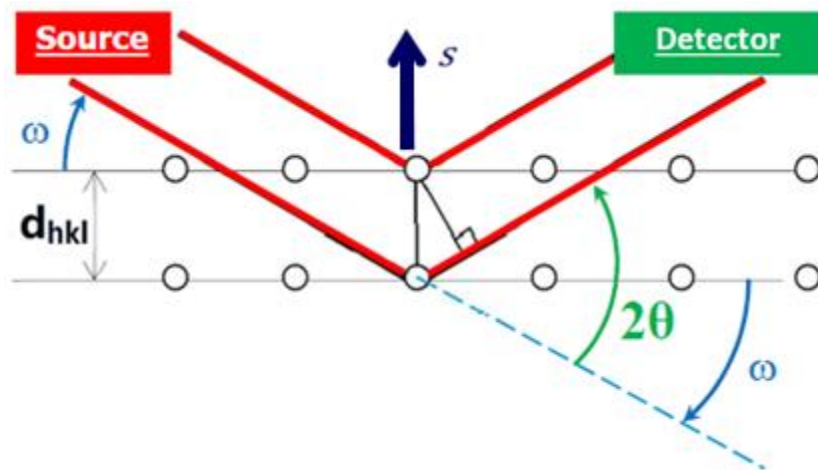
Figure 1 - 1D representation of the Bragg's law application.

2.2. Relation between diffraction and elastic strain

Diffraction uses the crystallographic structure of phases as strain gauge to measure the elastic strain. When a crystal is loaded (external or internal stress) its lattice parameters change. Therefore, the d-spacing changes from $d_0^{\{hkl\}}$ to $d^{\{hkl\}}$, resulting in a shift of the measured diffraction peak, see Fig. 2.
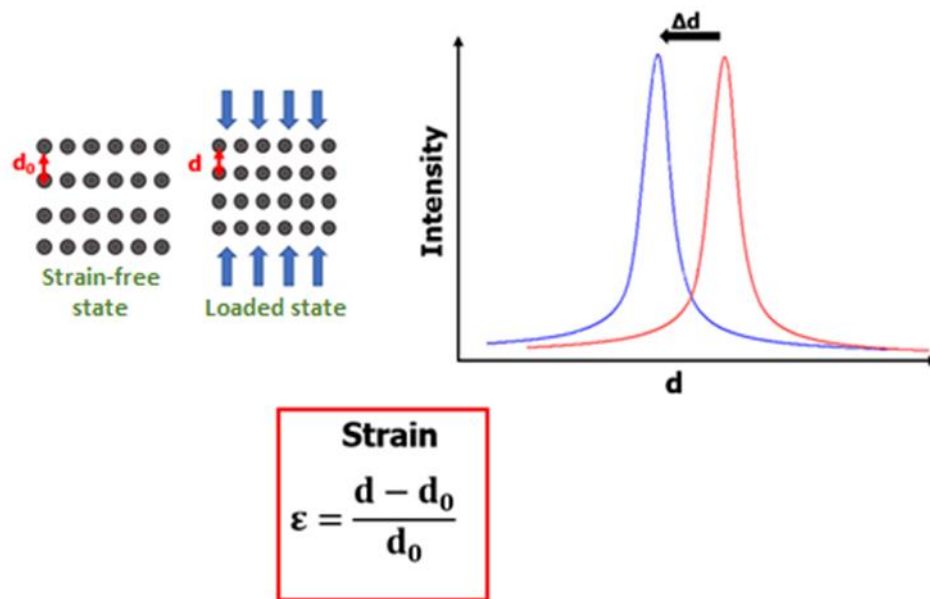
Figure 2 - Relation between interplanar distance and elastic strain.

The strain measured by diffraction, i.e. the variation of the interplanar spacing compared to a reference state (strain-free state) described in Eq. 3, represents a projection of the strain tensor in the measurement direction. The measurement direction is defined by the direction of the scattering vector. The scattering vector $\vec{q_s}$ is defined as the bisector between the incident and the diffracted beam, see Fig. 3. The scattering vector can be defined in the sample reference (S_1, S_2, S_3) using the angles ϕ and ψ, as represented in Fig. 4. The mathematical formulas defining the scattering vector and relating the strain measured by diffraction to the strain tensor in the specimen reference are given in Eq. 4 and Eq. 5, respectively.
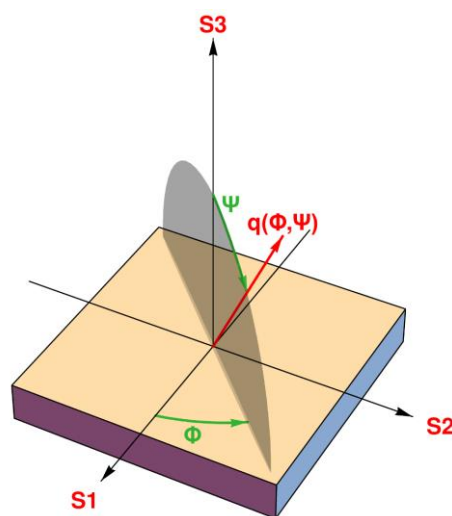
Figure 3 - Schematic representation of the measurement direction as defined by the direction of the scattering vector $\vec{q_s}$.

$$\varepsilon_q^{\{hkl\}} = \frac{d_q^{\{hkl\}} - d_0^{\{hkl\}}}{d_0^{\{hkl\}}} \qquad \text{Eq. 3}$$

$$\overrightarrow{q_s} = \begin{pmatrix} \cos\phi\,\sin\psi \\ \sin\phi\,\sin\psi \\ \cos\psi \end{pmatrix} \qquad \text{Eq. 4}$$

$$\varepsilon_{\phi\psi}^{\{hkl\}} = \varepsilon_{11}\cos^2\phi\,\sin^2\psi + \varepsilon_{12}\sin 2\phi\,\sin^2\psi + \varepsilon_{22}\sin^2\phi\,\sin^2\psi \qquad \text{Eq. 5}$$
$$+ \varepsilon_{13}\cos\phi\,\sin 2\psi + \varepsilon_{23}\sin\phi\,\sin 2\psi + \varepsilon_{33}\cos^2\psi$$

A more generalized definition of the direction of the measurement, i.e. the scattering vector, can be accomplished with five unique angles. Three angles are used to define the orientation of the specimen in the space, and the remainder to describe the position of the incident and diffracted beams (see Fig. 4). Therefore, two reference systems have to be defined: The sample reference system (S_1, S_2, S_3) and the goniometer reference system (G_1, G_2, G_3), see Fig. 4.

The sample reference system is defined as following:

- S_3 is normal to the surface of the sample and directed outwards.
- S_1 is in the plane of the surface and freely chosen by the operator. It is often selected parallel to a physically meaningfully direction, such as the rolling direction, the machining direction or the welding direction, etc.
- S_2 is chosen consequently so that the (S_1, S_2, S_3) system results conveniently positive within the gauge volume (GV).

The goniometer reference system is defined as follows:

- G_1 is parallel to the incident X-ray or neutron beam and directed in the direction of the propagation of the photons/neutrons.
- G_2 is parallel to the axial direction of the goniometer.
- G_3 is chosen so that the (G_1, G_2, G_3) system is direct.

The incident and diffracted beams, i.e. direction of the photons/neutrons, are defined by:

- The diffraction angle 2θ.
- The azimuth angle η that define the position of the diffracted beams along the Debye-Scherrer ring.

The three successive rotations that allow bringing the specimen from the reference position to the direction of the measurement, i.e. orientate the sample in space, are defined as follow (see Fig. 4):

- A rotation by φ around $-G_3$.
- A rotation by χ around G_1.
- A rotation by ω around $-G_2$.

At the reference position, $\varphi = \chi = \omega = 0$, the two reference systems are superposed. Multiple definitions and their correspondent mathematical formulas are available in the literature (He, 2009) (François, 2008) (Gelfi, 2004). They can be used as given or could be customized for an easier use depending on the beamline or the experimental apparatus. The general mathematical formulas

defining the direction of the scattering vector $\overrightarrow{q_s}$ and the measured strain $\varepsilon_q^{\{hkl\}}$ as a function of the strain tensor components are presented in Eq. 6 and Eq. 7, respectively. All the particular acquisition strategy, e.g. chi method, omega method, etc., can be derived from the general definition shown in Fig. 4 and its correspondent mathematical formulas.

$$\overrightarrow{q_s} = \begin{pmatrix} c\,\theta\,c\,\chi\,s\,\delta\,s\,\varphi + c\,\delta\,c\,\theta\,(-c\,\omega\,s\,\varphi\,s\,\chi + c\,\varphi\,s\,\omega) - s\,\theta\,(c\,\varphi\,c\,\omega + s\,\varphi\,s\,\chi\,s\,\omega) \\ -c\,\theta\,c\,\varphi\,c\,\chi\,s\,\delta + c\,\delta\,c\,\theta\,(c\,\varphi\,c\,\omega\,s\,\chi + s\,\varphi\,s\,\omega) - s\,\theta\,(c\,\omega\,s\,\varphi - c\,\varphi\,s\,\chi\,s\,\omega) \\ c\,\delta\,c\,\theta\,c\,\chi\,c\,\omega + c\,\theta\,s\,\delta\,s\,\chi + c\,\chi\,s\,\theta\,s\,\omega \end{pmatrix}$$

Eq. 6

Note: where "*c*" is the cosine function and "*s*" the sine function.

$$\varepsilon_{\phi\psi}^{\{hkl\}} = \varepsilon_{11}q_{s1}^2 + \varepsilon_{22}q_{s2}^2 + \varepsilon_{33}q_{s3}^2 + 2\varepsilon_{12}q_{s1}q_{s2} + 2\varepsilon_{13}q_{s1}q_{s3} + 2\varepsilon_{23}q_{s2}q_{s3}$$

Eq. 7

Figure 4 - Definition of the reference systems and the angles defining the measurement direction.

2.3. Relation between strain and stress

The stresses are related to the strains via the generalized Hooke's law. Knowing the elasticity constants of the analysed crystallographic plane (or the macroscopic elastic constants if first order peaks are averaged), the stresses can be calculated from the measured strains. The strain and stress in a component are defined using a second rank tensor. Therefore, to determine the full tensor at least six independent components, i.e. six independent measurement directions, of the strain tensor are required. It is recommended that the probed directions are sufficiently sensitive to the six components of the strain and stress tensors. However, for an orthogonal stress-strain measurement in an isotropic

material, stresses can be inferred if at minimum three strain components are measured, irrespective if their directions not being aligned with that of the principal. If the principal stress directions are known beforehand, strain measurements in the principal directions are sufficient to calculate the principal stress components; however, this rarely occurs in practice. Indeed, relative stress magnitudes in different orientations are sometimes known, but the specific invariants and their orientations rarely are.

2.4. Diffraction geometries

Different diffraction geometries may be used. In the following, the two used for residual stresses measurements are described.

2.4.1. Reflection geometry

It is the type of diffraction in which the incident and the recorded diffracted beams enter and exit from the same surface of a specimen. A schematic representation of diffraction within reflection geometry is shown in Fig. 5.
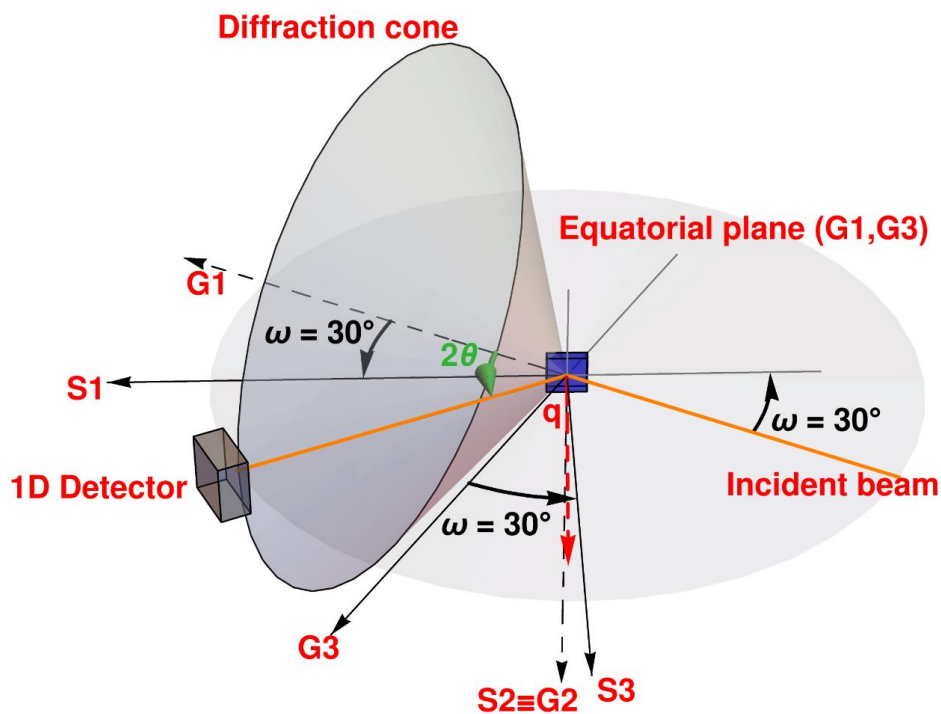
Figure 5 - Schematic representation of diffraction within reflection geometry.

2.4.2. Transmission geometry

It is the type of diffraction in which the incident and the recorded diffracted beams enter and exit from different surfaces of a specimen. A schematic representation of diffraction within transmission geometry is shown in Fig. 6.
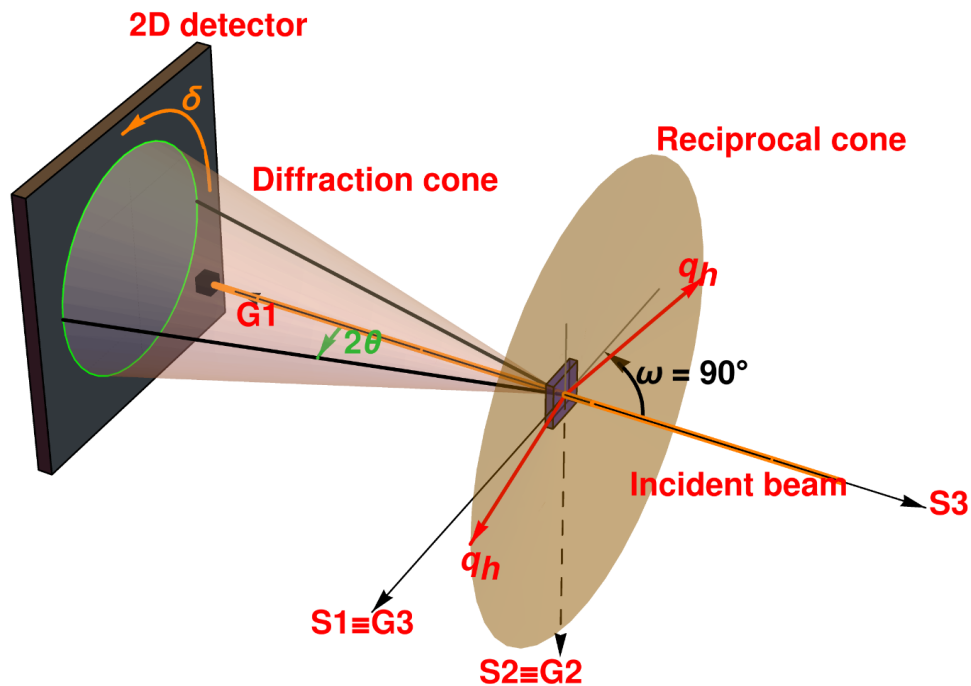
Figure 6 - Schematic representation of diffraction within transmission geometry.

3. Diffraction techniques

Both main features and the particularities associated with each technique are addressed in the following sections. At the end of this section, a summary presenting the best technique for each need, is presented.

3.1. High-energy X-ray diffraction

Synchrotron radiation facilities offer the possibility to study residual stresses in the bulk of thick components. The high intensity, flux, collimation, and wavelength tunability of the radiation allow instruments to provide performance and flexibility, which surpass what is possible with conventional laboratory apparatus. Instruments operating with a monochromatic beam (i.e. using angular dispersive set-up) or a polychromatic beam (i.e. using energy-dispersive set-up), are available at different synchrotron facilities. The general properties of synchrotron radiation include (Fitch, 2019):

- High brightness, i.e. a highly collimated, intense X-ray beam and small source size, which cannot be achieved by conventional laboratory X-ray instruments.
- High flux of photons delivered to the sample.
- A range of wavelengths is available, extending from the soft to the hard X-ray energies depending on the facility.

More information about synchrotron radiation can be found elsewhere in the literature (Fitch, 2019) (Als-Nielsen, 2011) (Mobilio, 2015).

3.1.1. Polychromatic beam for energy-dispersive X-ray diffraction

In energy-dispersive X-ray diffraction (EDXRD) the white beam as originally obtained from synchrotron sources is used. The diffracted beam is recorded using solid-state semiconducting detectors. In this type of setup, the diffraction angle is fixed and a wide range of energy spectra is used. Using EDXRD a complete diffraction pattern is obtained at a constant diffraction angle, through the use of an energy dispersive detector. This allows reducing the time of the experiments, when being compared to experiments carried out with a monochromatic beam coupled with point or linear detectors that need to scan the whole 2θ range to record the whole diffraction pattern. For strain measurement, a set-up with two different detectors is often used that allows measuring the strain in two independent directions reducing the measurement time. Using this set-up, a gauge volume can be easily defined in the bulk of the sample using a set of slits. Therefore, maps of residual strains and stresses can be built by translating or rotating the sample in the directions parallel and perpendicular to the beam, measuring the d-spacing evolution compared to a reference d-spacing value at different sample positions and, finally, rotating the sample by 90° to measure the remaining strain and calculate the stresses.

a. Principal components of an EDXRD set-up

The principal components of the EDXRD set-up are wiggler, slits, sample stage and cradles, detectors, cooling system, and electronics. A schematic presentation of the set-up is shown in Fig. 7.

- Wiggler: insertion device used to produce a very intense synchrotron radiation with a wide range of energy spectra and high flux.
- Primary slits: slits situated in the optics hutch. They are used to select a primary beam size in order to obtain a certain beam size in the experimental hutch.
- Sample stage and cradles: generally, it consists of a table on which the sample is clamped for the measurement. It allows translating and rotating the sample in different directions to bring it to the desired spatial position and measurement direction for stress mapping. Different tools, i.e. Eulerian cradle and heavy load diffractometer, are often available at the facilities allowing the manipulation of samples with different dimensions and weights.
- Secondary slits: are situated in the experimental hutch and are used to give the final shape to the beam (S1 and S2 in Fig. 7).
- Detector slits: pair of slits (S3 and S4 in Fig. 7), one after the sample and the other before the detector, fixed at a scattering angle 2θ. Their intersection with the incident beam defines the gauge volume.
- Detector: solid-state semiconducting detectors are used to record the diffraction pattern. The signal generated from the interaction between the diffracted photons and the semiconductor crystal is converted to a digital signal and processed with multi-channel analysers (MCA) or digital signal processors (DSP).
- Cooling system: used to maintain the detectors temperature to work in optimum conditions.
- Electronics: used to process and filter the signal and give the final diffractogram as channels as a function of number of counts/events. The main components of the electronics of the detector are preamplifier, digital signal processor, multi-channel analyser, and high voltage supplier.
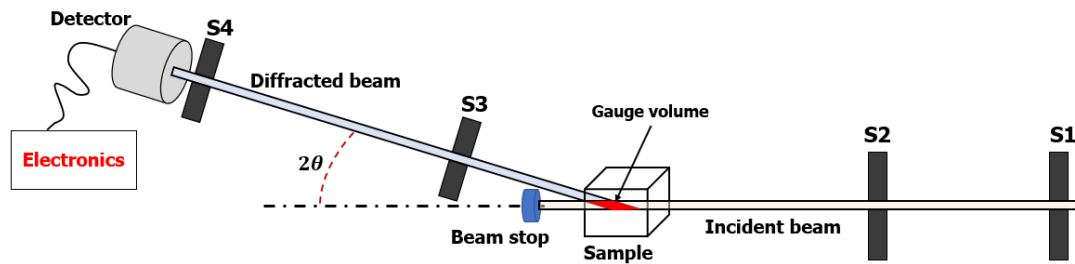
Figure 7 - Schematic presentation of the EDXRD experimental set-up.

b. Energy range

The energy spectrum band used in EDXRD is dependent on the facility. Generally, an energy spectrum between 20 and about 300 keV is used for strain measurement on metallic components.

c. Gauge volume definition – Transmission mode

The gauge volume is defined as the intersection between the incident beam and the projection of the detector slits (see Fig. 7 and Fig. 8). The use of a high energy (small wavelengths) results in a small scattering angle. As a consequence, the gauge volume shape is not cubic but a rhombic prism elongated in the direction of the beam as it can be seen in Fig. 7 and Fig. 8.
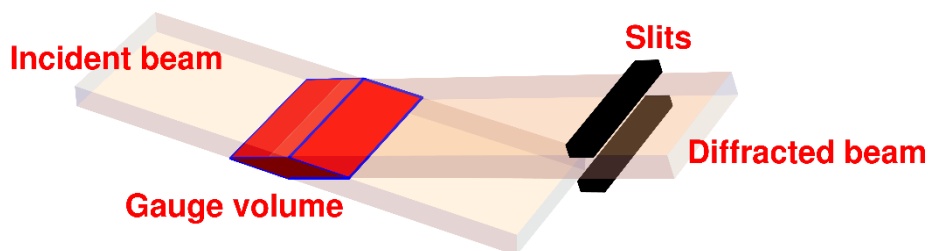
Figure 8 - Gauge volume as defined by the intersection between the incident beam and the slits.

The gauge volume size can be estimated from the beam size and the detector slits opening. Generally, the dimension of the gauge volume in the beam direction is elongated by a factor of about 10 compared to the beam size. An illustrative example of the dimension of the gauge volume in the beam direction is represented as a function of the beam size (square beam) for a diffraction angle $2\theta = 5°$ and detector slits with an opening of $100 \ \mu m$ in **Error! Reference source not found.** 9.
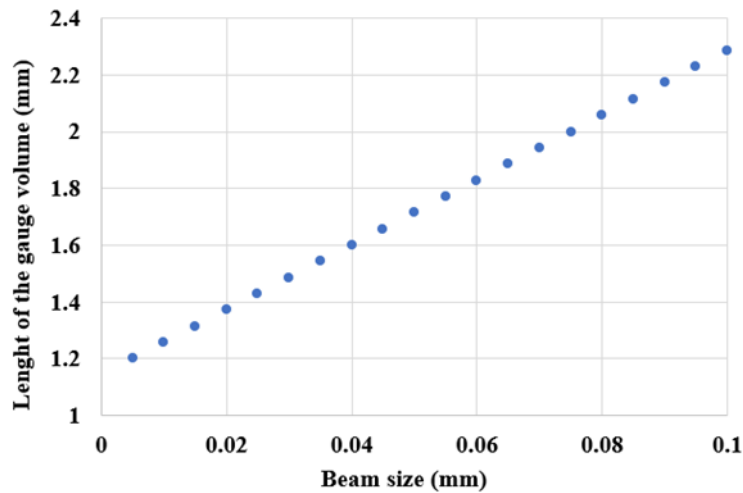
Figure 9 - Length of the gauge volume in the beam direction as a function of the beam size (square beam) for a diffraction angle $2\theta = 5°$ and back and front detector slits with an opening of $100\ \mu m$.
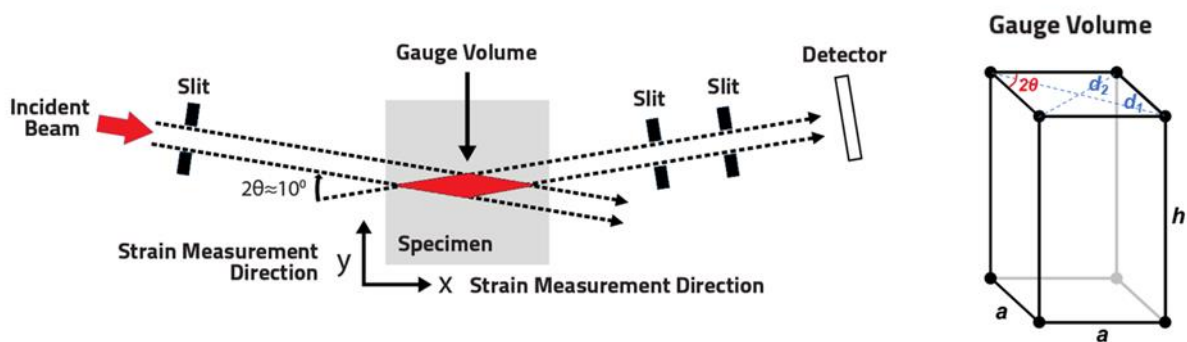
Figure 10 - Gauge volume as defined by the intersection between the incident beam and diffracted beam and its schematic representation.

According to Fig. 10 showing the gauge volume schematic representation, its main features are easily calculated. The gauge volume Vol_G is a parallelepiped with two rhombus bases of the prism, defined by Eq. 8 as the rhombic area $A_{rhombic}$ multiplied by the beam width, corresponding to the prism height h.

$$Vol_G = A_{rhombic} * h$$

Eq. 8

The rhombic area $A_{rhombic}$ is given by Eq. 9, in which are described the relation between the diagonals d_1 and d_2 , the diffraction angle 2θ and the edges a.

$$A_{rhombic} = a^2 * \sin 2\theta = \frac{d_1 * d_2}{2}$$

Eq. 9

Further, all the features describing the rhombic area may be related to the slit aperture s through trigonometric relationships, reported in Eq. 10, Eq. 11, Eq. 12:

$$d_1 = \frac{s}{\sin\theta}$$ *Eq. 10*

$$d_2 = s * \cos\theta$$ *Eq. 11*

$$a = \frac{d_1 * \cos\theta}{2}$$ *Eq. 12*

The feature describing the rhombic area corresponds also to those describing the gauge volume. Indeed, the gauge volume length corresponds to the major diagonal d_1, the gauge volume height corresponds to the minor diagonal d_2 and, as stated previously, the gauge volume width corresponds the incident beam width.

Further, more information on the calculation of the dimensions of the gauge volume can be found elsewhere (Rowles, 2011) (Reimers, 2008).

d. Gauge volume definition – Reflection mode

Energy dispersive diffraction can also be done in reflection mode. In this configuration, the incident beam illuminates the surface of the sample at an angle, similarly to what is done in lab X-ray methods (Fig. 11).
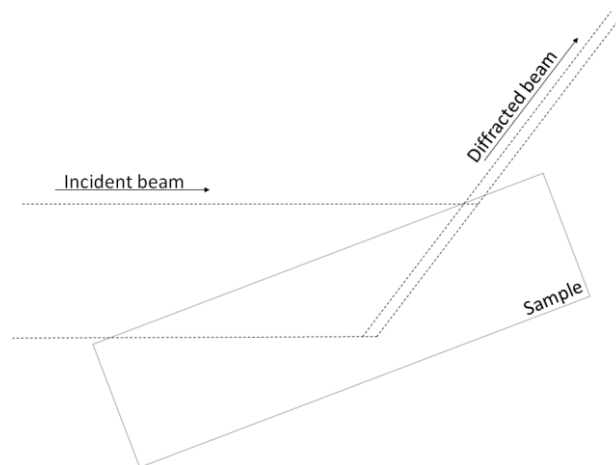
Figure 11 - Schematic representation of energy dispersive reflection mode.

On such illumination condition, each energy will have a different penetration depth in the material. Since several peaks are measured simultaneously, it is possible to analyse each peak independently. The data yielded by each peak will correspond to the average behaviour of the material through depth convolved with an exponential decay given by the absorption of the beam in the material. Since each

energy has a different absorption coefficient, the convolved result will be different for each peak. In this sense, reflection geometry can be used to probe surface gradient properties.

On the surface of the sample, the gauge volume is defined by the region of the sample bathed by the beam. Many applications require rotation of the sample, so changes in beam footprint must be considered when designing an experiment. The thickness gauge volume definition is typically done considering the attenuation length resolved against energy for the analysed material. The attenuation length τ is defined as the thickness at which the ratio between transmitted intensity I and the incident intensity I_0 equals e^{-1}, or the inverse of the energy dependent mass absorption coefficient μ.

$$\frac{I}{I_0} = e^{-\mu\tau} = e^{-1} \therefore \tau = \frac{1}{\mu} \qquad \text{Eq. 13}$$

During a measurement, the incidence geometry can also affect the penetration depth t of the beam. Since the beam arrives at an angle, the penetration depth will be a fraction of the attenuation length. The equation below describes the variation of penetration depth depending on the sample rotational coordinates:

$$t = \frac{((\sin\omega^2 - \sin\psi^2 + (\cos\omega^2 * \sin\psi^2 * \sin\eta^2))}{(2\mu\sin\omega * \cos\psi)} \qquad \text{Eq. 14}$$

On an energy dispersive reflection experiment, 2θ can be adjusted to position the materials diffraction peaks in energies which cover a specific depth region. This way, the depth of interest can be chosen for each sample. For example, the Fig. 12 below shows the energy for austenitic and ferritic steel peaks resolved against 2θ. The colour scale indicates the penetration depth for a specular condition ($\omega=2\theta/2$).
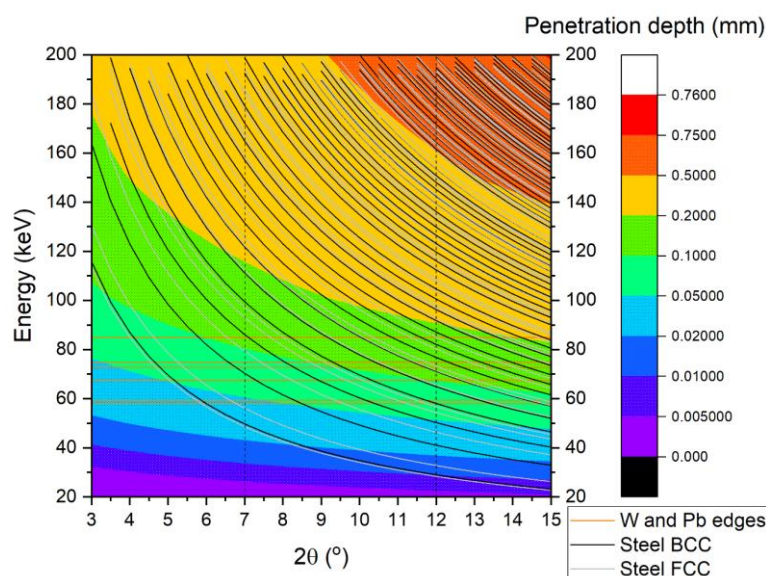
Figure 12 - Energy position vs 2θ for austenitic and ferritic steels on energy dispersive diffraction. The colour scale indicates the penetration depth on specular reflection. The dashed vertical lines indicate most commonly used operation range at P61A. Tungsten and Lead fluorescence lines are typically present on the collected data and are also shown.

The correlation of energy dispersive reflection data with penetration depth can be done in multiple ways. Some methods of note are the universal plot and the white beam multiwavelength methods. In universal plot, a penetration depth is assigned to each peak collected at each position, and the measured d-spacing is plotted against orientation or depth for all data. In the white beam multiwavelength method, measured peak positions are grouped together based on hkl values, and a single penetration depth is assigned for each group. Within each group, results from different orientations are analysed together with d-spacing vs $\sin^2\psi$ plots.

Once stresses have been determined against penetration depth, the stress gradient can be deconvolved from the absorption exponentials by using an inverse Laplace transform.

3.1.2. Monochromatic beam for angle-dispersive X-ray diffraction

The polychromatic beam is filtered by passing it through a perfect highly oriented crystal, i.e. a monochromator. The diffracted beam is recorded using $0D$, $1D$, or $2D$ detectors. Nowadays, the facilities are equipped with $2D$ detectors, which reduce significantly the measurement time, avoiding the 2θ range scanning and sample orientation, needed, when a $0D$ or $1D$ detectors are used. Strain measurements can be done on 2-dimensional samples, e.g. a foil, without the definition of a gauge volume. In order to map the strain/stress in the bulk of thick samples, a gauge volume can be defined using conical or spiral slits (Lienert, 2000) (Martins, 2003) (Martins, 2005). Therefore, a map of residual strain/stress can be built by translating/rotating the sample in the directions parallel and perpendicular to the beam and measuring the d-spacing evolution compared to a reference d-spacing value at different sample positions.

a. Principal components of an angle dispersive X-ray diffraction (ADXRD) set-up

The principal components of the angle dispersive X-ray diffraction (ADXRD) set-up are: undulator, monochromator, slits, focusing optics, sample stage and 2D detector. Some beamlines are equipped with conical slits and/or spiral slits. A schematic representation of the set-up is shown in Fig. 13. The main components are described below:

- Undulator: insertion device used to produce a very intense synchrotron radiation with a very narrow energy bandwidth.
- Monochromator: it consists of one or a pair of perfect crystals set to a particular angle to the incident beam. The perfect crystal acts like a filter and only pass the wavelength that satisfies the Bragg's condition. Nowadays, almost all of the beamlines are equipped with monochromators able to deliver an X-ray beam with an energy resolution of $\frac{\Delta E}{E} \leq 10^{-4}$.
- Primary slits: slits situated in the optics hutch. They are used to give a primary shape to the beam.
- Focusing optics: allows to focus the beam to the desired dimensions. They can consist of lenses, mirrors, etc.
- Secondary slits: are situated in the experimental hutch and are used to give the final shape to the beam.
- Sample stage and Eulerian cradle: it consists of a table on which the sample is clamped for the measurement. It allows to translate and rotate the sample in different directions to bring it to the desired spatial position and measurement direction for stress mapping. Different tools are

often available at the facilities, allowing the manipulation of samples with different dimensions.

- $2D$ detector: area detector that allows to record the whole diffraction rings. Often two-dimensional detectors with a flat detection surface are used. Several types of detectors offering different advantages are available at the facilities, e.g. photon-counting detector, charge-coupled device (CCD) detector, etc.
- Conical or spiral slits: It consists of a plate on which narrow rings with micrometric apertures are machined. The conical aperture intersects the diffracted beam from the sample and defines a gauge volume in the bulk of the material. More information about conical and spiral slits can be found elsewhere in the literature (Lienert, 2000) (Martins, 2003) (Martins, 2005).
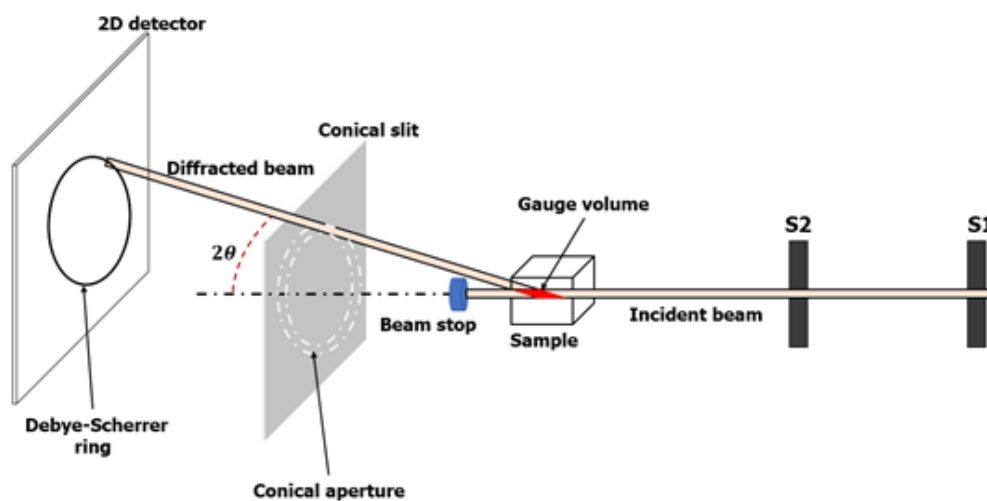
Figure 13 - Schematic presentation of the ADXRD experimental set-up with a conical slit cell.

b. Gauge volume

The gauge volume is defined as the intersection between the incident beam and the projection of the aperture slits (see Fig. 13). The use of a high energy (small wavelength) results in a small scattering angle as is the case for EDXRD. As a consequence, the gauge volume is not homogeneous in all directions but elongated in the direction of the beam. The diffraction angle is not fixed and the gauge volume probed in the sample is not the same for the different $\{hkl\}$ planes. The length of the gauge volume is inversely proportional to the diffraction angle and can be calculated as a function of the beam size, aperture size, distance between sample and slit, diffraction angle, distance between slit and detector and the resolution of the detector. More information can be found elsewhere in the literature (Lienert, 2000).

3.2. Neutron diffraction

Neutron diffraction uses beams generated by either fission or spallation. In both cases the used neutrons have wavelengths bigger than $0.05 \, nm$. Monochromatic or Time-of-Flight (TOF) type instruments are used for strain measurement. Actually, in this project only monochromatic instruments have been used.

3.2.1. Monochromatic instrument

A monochromatic instrument uses a monochromatic beam. For that aim, the polychromatic neutron beam is filtered by passing it through a perfect highly oriented crystal, i.e. a monochromator. The diffracted beam is recorded using a neutron detector. A gauge volume can be defined in the bulk of the sample using slits and/or collimators. Again, to obtain a map of residual strain/stress the sample has to be translated in the directions parallel and perpendicular to the beam and the d-spacing evolution compared to a reference d-spacing value at different sample position have to be measured.

a. Principal components of a neutron monochromatic instrument

The main components of a neutron monochromatic instrument set-up are: monochromator, beam shaping optics, sample stage, and detector. A schematic drawing of the set-up is given in Fig. 14.

- Monochromator: it consists of a set of single crystals in a particular angle to the incident beam to select a proper wavelength.
- Beam shaping optics: radial collimators and/or slits used for gauge volume definition, both on the incident beam and the diffracted beam sides.
- Sample stage: There are different options for sample stages such as xyz-table, Eulerian cradles, hexapod, etc., Generally, it consists of a device on which the sample will be clamped for the measurement. It allows to translate and rotate the sample in different directions to bring it to the desired spatial position and measurement direction for stress mapping. A range of sample stages exist, that allows the different neutron facilities the manipulation of samples with different dimensions and masses.
- Sample alignment system: system which is typically based on mechanical or optical probes that aid with the initial positioning and alignment of the sample with respect to the reference point.
- Neutron detector system: A system that records the diffracted neutron intensities as a function of angle or time-of-flight. The detector angular position with respect to the incident beam define the geometry of the gauge volume and the scattering vector, i.e. the measurement direction. Similar to the previously described XRD section, there are also for neutrons different types of detectors available (Oed, 2004).
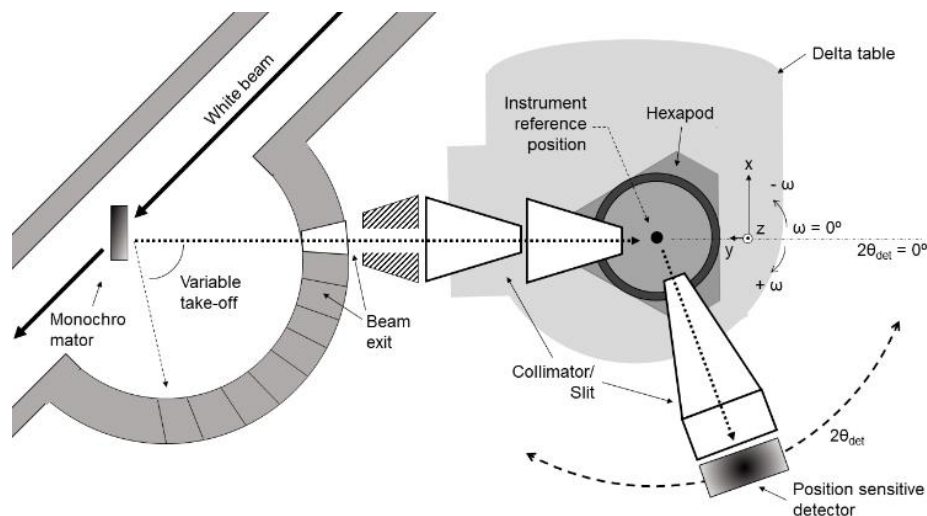
Figure 14 - Schematic presentation of a monochromatic neutron diffraction instrument. This specific example represents the strain mapping instrument SALSA at ILL.

b. Instrument gauge volume

Due to the available neutron wavelengths of $\lambda \geq 0.05$ nm, diffraction with an angle of 90° can in most cases be obtained, allowing a cubic gauge volume within the bulk of the material (see Fig. 15). However, this is not always the case and depending on the material, the GV can also be rhombohedral. The size and dimensions of the GV can be calculated in a similar manner as shown above under 3.1.1c.
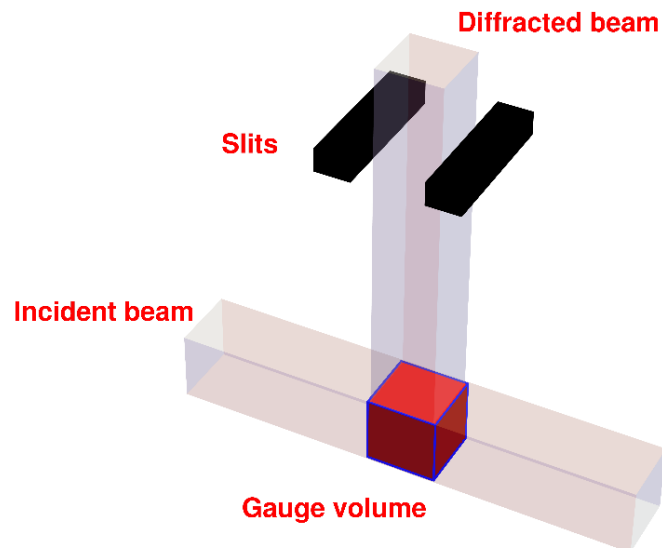
Figure 15 - Instrument gauge volume as defined by the intersection between the incident beam and the slits in the diffracted beam.

3.3. Laboratory X-ray diffraction

Residual stress analyses by X-ray diffraction in a laboratory are carried out with diffractometers such as X-Raybot, Set X or Bruker following the EN 15305 (2009) standard: Test methods for residual stress analysis by X-ray diffraction (EN15305:2009).

The X-ray diffraction peak acquisitions are defined as follow in Tab. 1 for a b.c.c. steel component (the X-ray tube will change as a function of the characterized material).

Table 1 - Laboratory X-ray diffraction main features.

Installation	X-RAYBOT UR5 V2
Detector	Linear
Linear	ψ
Radiance	Kα of Chrome
Kβ filter	Vanadium
Wavelength	2.29 Å
Counting time	150 s per exposure angle ψ

Current / Tension	20 kV / 1mA
Theoretical peak position	156° in 2θ
Collimator	2 mm
13 ψ angles	from -37° to 39°
Oscillations	No
Using Masks	Yes

For each defined material, the X-ray crystallographic constants are defined as present for the steel and the crystal plane (2 1 1) reported in Tab. 2.

Table 2 - X-ray cristallographic constants are defined as present for the steel and the plan (2 1 1).

$h-k-l$	**2 1 1**
½S2	5.83 * 10^{-6} MPa^{-1}
S1	-1.28 * 10^{-6} MPa^{-1}

3.4. EASI-STRESS available techniques compendium

In the following table, the main features of the residual stress measurement techniques available in the EASI-STRESS project are listed (Tab. 3), in order to help choosing the right technique that satisfies the specific needs of the use.

Table 3 - Main features of the residual stress measurement techniques available in the EASI-STRESS project.

Feature	EDXRD (ESRF)	EDXRD (Hereon)	ADXRD (ESRF)	ADXRD (Hereon)	ND (ILL)	ND (ATHOS)
Sample Weight [kg]	<10 Cradle; <500 Stage	<40 Cradle; <1000	<20 Stage	<1000 Hexapod	<50 Cradle; <1000 Hexapod	<40 Stage
Sample Surface Finish	None	None	None	None	None	None
Sample safety issue rejection (e.g. Radioactivity)	Yes	Yes	Yes	Yes	No	No

Measured Gauge Volume Shape	Rhombic prism (~2D)	Rhombic prism (~2D)	Rhombic prism (~2D)	Rhombic prism (~2D)	From Cubic (3D) to rhombic prism (~2D)	From Cubic (3D) to rhombic prism (~2D)
Measured Gauge Volume - Edge a [mm]	0.005 - 1,8	0.05 - 1	0.05 - 3	0.005 - 1	0.6, 2, 4, 10, 20	2 - 10
Measured Gauge Volume - Edge b [mm]	0.005 - 1,8	0.05 - 1	0.05 - 3	0.05 - 1	0.6, 2, 4, 10, 20	2 - 10
Measured Gauge Volume - Edge c [mm]	0.028 - 0.1	0.5 - 5	0.05 - 2	0.5 - 5	0.6, 2, 4, 10, 20	2 - 10
Measured Gauge Volume – Diffraction Angle α = 2θ [°]	6 - 14°	5 - 15°	~10	0 - 20°	55° - 125°	60° - 110°
Measured Gauge Volume - Max Depth [mm]	7 cm Al, 2,5 cm steel	4 cm steel	7 cm Al, 2,5 cm steel	8 cm Al, 2 cm steel	20 cm Al, 3 cm Fe, 4 mm Ti	10cm Al, 2cm Fe
Measure Error [MPa]	5 - 50	5 - 50	5 - 50	5 - 50	10 - 50 (depending on material)	100 – 300 (depending on the measurement time)
Measure Spatial Resolution [mm]	0.001		0.001		0.5 - 1	2 - 10
Beam Energy [keV]	20 - 140	20 - 300	6 - 80	40 - 150	$0.3 - 3 \times 10^{-3}$	$2 - 6 \times 10^{-6}$

4. **Technical specifications of the different diffraction instruments**

Diffraction methods are widely used for the non-destructive characterization of residual stresses in polycrystalline materials. The building of instruments optimized for engineering applications at the different large-scale facilities made it possible to investigate residual stresses inside industrial components non-destructively. The basis of diffraction techniques, using high energy X-rays or thermal neutrons, is to determine the evolution of the crystallographic parameters of the polycrystalline material compared to a reference state. By probing the evolution of the crystallographic parameters in the 3 dimensions of the space, a map of residual stresses inside the sample can be produced with a millimetric to micrometric spatial resolution. In the following, the different instruments available at the different large scales facilities that are involved in the EASI-STRESS European project are described.

4.1. X-ray techniques

4.1.1. ID15A energy dispersive diffraction setup at ESRF

The energy-dispersive diffraction set-up installed at ID15A (Insertion Device) uses a polychromatic beam covering a wide energy spectrum. That allows to collect multiple diffraction peaks simultaneously using a fixed, but arbitrary diffraction angle. Using this technique, a strain in a specific direction can be calculated using one diffraction peak or the whole collected diffraction pattern. A gauge volume can be defined in the sample using a set of slits. Therefore, a map of residual strain/stress can be built by translating the sample in the directions parallel and perpendicular to the beam and measuring the d-spacing evolution compared to a reference d-spacing value at different sample positions. Fig. 16 shows the instrument with the different components used during a strain/stress mapping campaign.
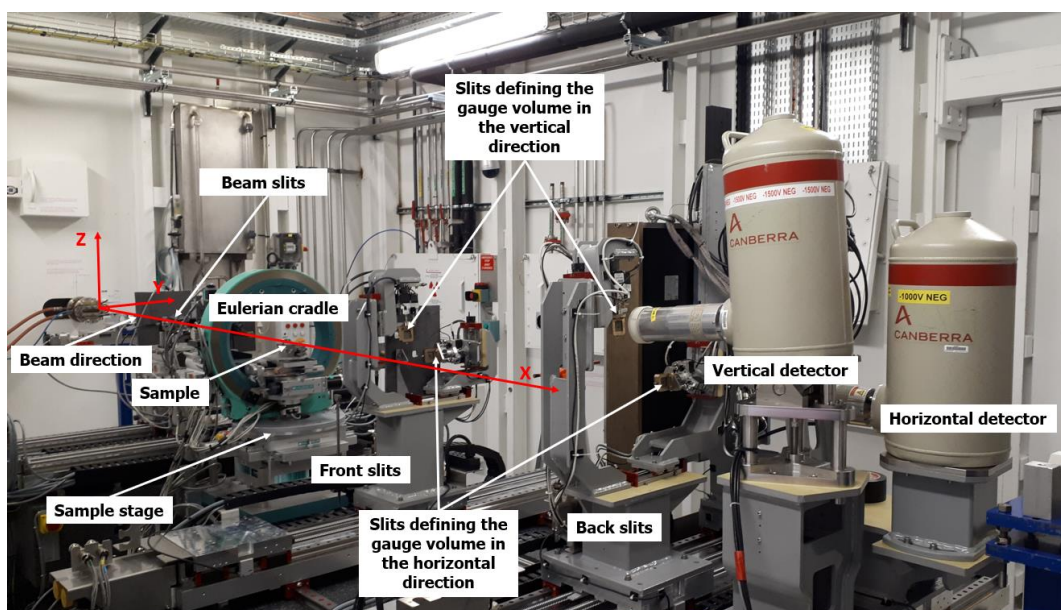
Figure 16 - Energy dispersive diffraction set-up installed at ID15A.

The main components of the instrument are:

- Wiggler: ID15A is equipped with a W76 wiggler able to provide white beam with energy between 20 and 500 keV. For most of metallic materials the range of used energy is between 50 and 300 keV. It allows to determine strain/stress in the bulk of thick metallic samples.
- Beam slits: two sets of pair of slits are used. The first pair is used to define the shape of the incident beam in the horizontal and vertical direction after a first collimation of the beam using primary optics. The second pair is often used to cut the reflection coming from the interaction of X-rays with the first pair of slits. The beam can be collimated down to 50 μm in the two directions. Beam collimation will influence the flux and the diffraction conditions. The beam size has to be adapted to the microstructure.
- Sample stage and cradles: the instrument is equipped with a sample stage providing by default three translations (T_x, T_y and T_z) and one rotation R_z. The different motor ranges are given in Tab. 4. The sample stage installed at ID15A can support up to 500 kg of load. A full-circle cradle, equipped with a translation stage, can be installed on top of the sample stage offering more degree of freedom for sample orientation. It allows to probe different directions in the space. It provides three translations (x, y and z) and two rotations (phi and chi). The different motor ranges are given in Tab. 5. The Eulerian cradle shown in Fig. 16 can support up to 10 kg of load. Different Eulerian cradles are available at ESRF and can be used depending on the need.

Table 4 - Motor stroke and resolution of the sample stage.

Motor	Travel	Resolution
T_x	200 mm	0.01 mm
T_y	1000 mm	0.01 mm
T_z	120 mm	0.01 mm
R_z	360 °	

Table 5 - Motor stroke and resolution of the Eulerian cradle shown in Fig. 16.

Motor	Travel	Resolution
x	150 mm	0.001 mm
y	150 mm	0.001 mm
z	20 mm	0.001 mm
Phi	360°	0.002° → 0.001°
Chi	360°	0.001°

- Front and back slits: they are used to define a gauge volume in the sample for each detector. The gauge volume size is dependent on the beam size and the slits opening. Due to the synchrotron high energy resulting in small scattering angles, the gauge volume is not homogeneous in all directions (like-diamond shape). The choice of the beam and slits size will define the spatial resolution in the three directions. The spatial resolution in the directions perpendicular to the beam is equal to the beam size. The length of the gauge volume (spatial resolution along the beam direction) is defined by the beam size and the slits opening. For illustration, the length of the gauge volume as a function of the beam size is shown in Fig. 9.

- Detectors: two Ge solid state detectors with a cylindrical shaped crystal (12 mm in diameter and 10 mm thickness) are used. The resolution of the detectors is dependent on the maximum energy and the number of channels settled in the multi-channel analyser (MCA) during the experiments. To give an example, the energy resolution is about 73 eV for a maximum energy of 300 keV and a number of channels equal to 4096. The detectors are fixed at a diffraction angle $2\theta = 5°$. The two detectors are positioned in the space to record two independent perpendicular strain components at the same time.

4.1.2. P61A White Beam Engineering Materials Science beamline at DESY-Hereon

The beamline P61A is optimized for residual stress measurements within the bulk (transmission mode) and near the surface (reflection mode). P61A is the first hutch of beamline P61, which is operated by Hereon (Fig. 17). In the downstream hutch P61B, DESY operates a large-volume press instrument for studies of materials under extreme conditions.

P61A focuses on energy dispersive diffraction experiments for Materials Science and Engineering. It is optimized for energy-dispersive residual stress measurements (P61A(a)) (P61A(b)). Small samples can be handled using a Eulerian cradle (Fig. 18), and a larger chi-circle used in combination with the heavy load diffractometer will become available in 2023. Two energy-dispersive solid-state detectors are used for stress measurements, whose positions define the scattering vector directions, one for each detector. The sample is scanned regarding this vector and diffractograms are collected for each point. These measurements can be performed both in transmission and reflection geometries (Fig. 19).
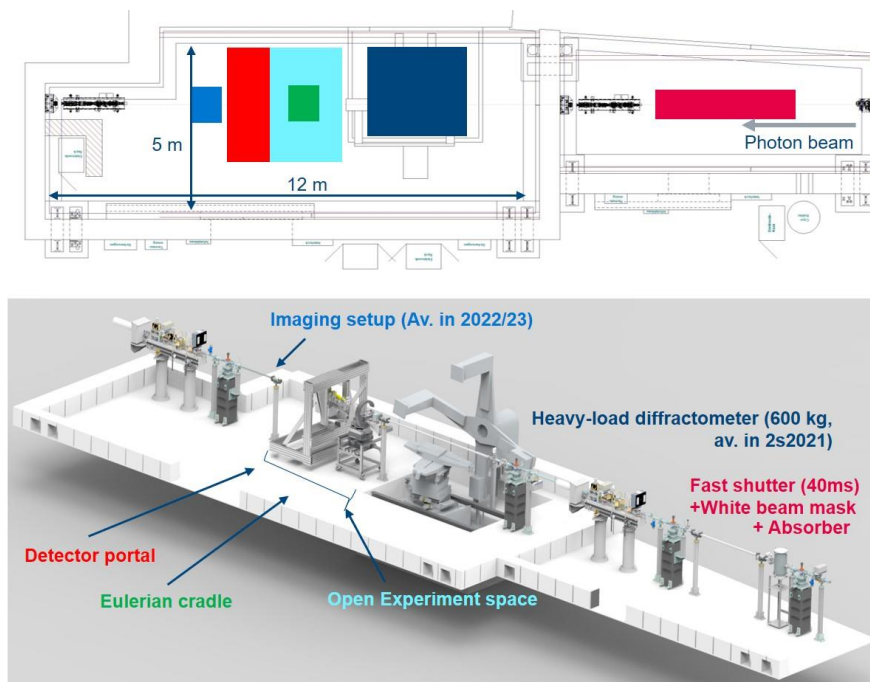
Figure 17 - P61A layout (Zenithal view top and 3D view bottom) with optics hutch (right side) and experiment hutch (left side).

Stress measurements are done using the $\sin^2\psi$ method. Scan macros and data reduction and analysis software are available at the beamline for both applications. Particularly in reflection geometries,

near-surface stress gradients can be determined by using Laplace space methods using the configurations presented in (Apel, 2018).

Figure 18 - P61A setup in the experiment hutch (beam coming from the right).
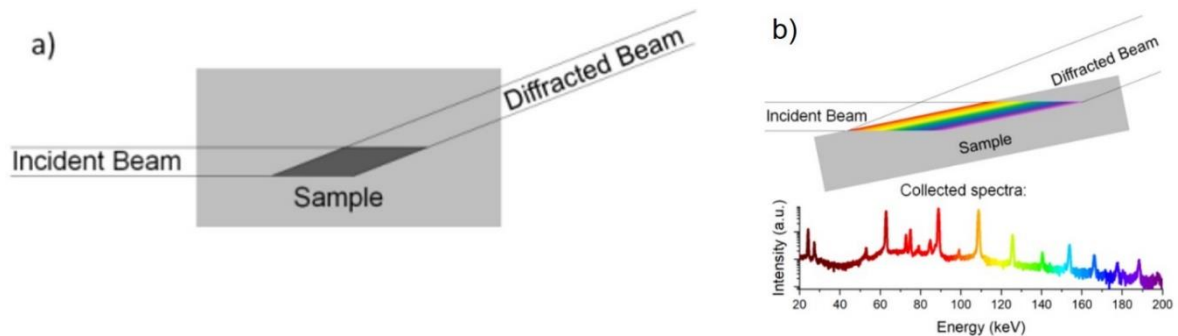
Figure 19 - Energy dispersive diffraction experiment in: a) transmission and b) reflection geometries.

The main components of the instrument are:

- Wiggler: the X-ray source of the beamline P61 (P61A(c)) is an array of ten 4 m long fixed-gap damping wigglers which serve to reduce the machine emittance. The powerful white beam from these insertion devices is filtered by an absorber unit to reduce the total power load on the downstream optical elements. The beam size is adjusted by a high-power slit system in the front end. The filtered white beam ("pink" beam) is then guided to the experimental hutches, which will employ energy dispersive X-ray techniques. The incident synchrotron radiation results in a high intensity beam of which energies from 30 to 200 keV are used (Fig. 20). The maximum source flux is 10^{12} ph/(s.mm^2.0.1% b.w.) at 50 keV, 100 mA, and 10^{11} ph/(s.mm^2.0.1% b.w.)at 200 keV, 100 mA.
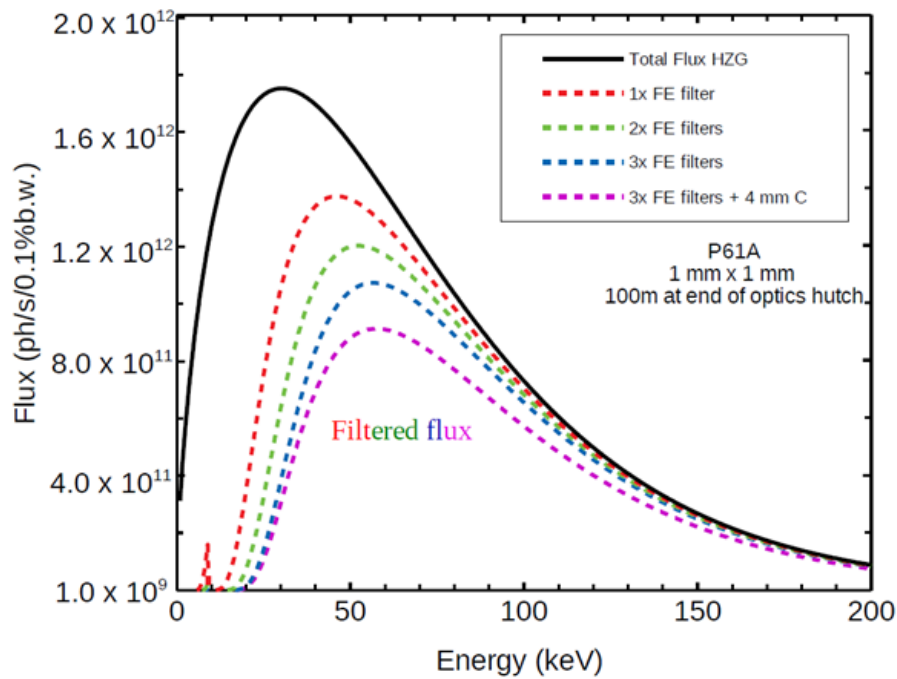
Figure 20 - Flux generated by the damping wigglers at the P61 beamline.

- Optics: the beam size can be shaped with slits apertures ranging from a minimum of 0.05 × 0.05 mm^2 to a maximum of 1.5 × 1.5 mm^2.
- Eulerian cradle: stress measurements on small samples are performed using the Eulerian cradle (Fig. 21), which enables the sample translation and/or rotation in all spatial directions to apply the sin$^2\psi$ method. The position accuracy is 2 μm with a load capacity of 5 kg. The specifications of the Eulerian cradle are detailed in Tab. 6.

Figure 21 - Eulerian cradle at the P61A beamline.

Table 6 - Eulerian cradle travel ranges.

Axis	Travel range
φ	360°
χ	160°
ω	5° (vert.), ± 25° (hor.)
θ	0-5.5°
x	150 mm
y	150 mm
z	25 mm

- Heavy load diffractometer: a heavy stage diffractometer with a load capacity of 600 kg is available at P61A (Fig. 22). It enables a versatile positioning of large sample environments with a movement range of 1 m × 1 m × 0.2 m. Measurements are performed with a large detector goniometer or a detector portal behind the diffractometer. Moreover, a 30 kg capacity χ stage is under design.

Figure 22 - Heavy load diffractometer at P61A.

- Detectors: During a stress measurement, the energy dispersive detector positions define spatially the scattering vector directions, one for each detector. Two high purity Ge-detectors (see Fig. 23 and Tab. 7 for technical specifications) can be used simultaneously and independently positioned at any azimuth angle with a 2θ between 0° and 12° and, therefore, the instrument is able to measure strains in two independent directions at the same time, reducing the number of measurements necessary for a stress scan. The detector range is 20 − 204 keV with 4096 channels and a resolution of 0.05 keV/channel. Both detectors are

equipped with 0.5 m long double slit collimators. The sample is scanned regarding this vector, and peak positions are collected for all energies at each point. These experiments can be performed in both transmission and reflection geometries. In reflection geometry, peaks from different hkl families are measured simultaneously at different energies on a fixed scattering vector direction. Since each energy has a different absorption coefficient, a probing depth can be assigned to each peak collected, which can be uniquely used to study near surface stress and microstructural gradients. Note that specific software is required to do data analysis in this case. A sketch of the Eulerian cradle axes nomenclature (Φ, χ, ω) together with the two-detector (D1, D2) setup for a measurement is shown in Fig. 24. The setup also allows for variation of angle of incidence (θ).
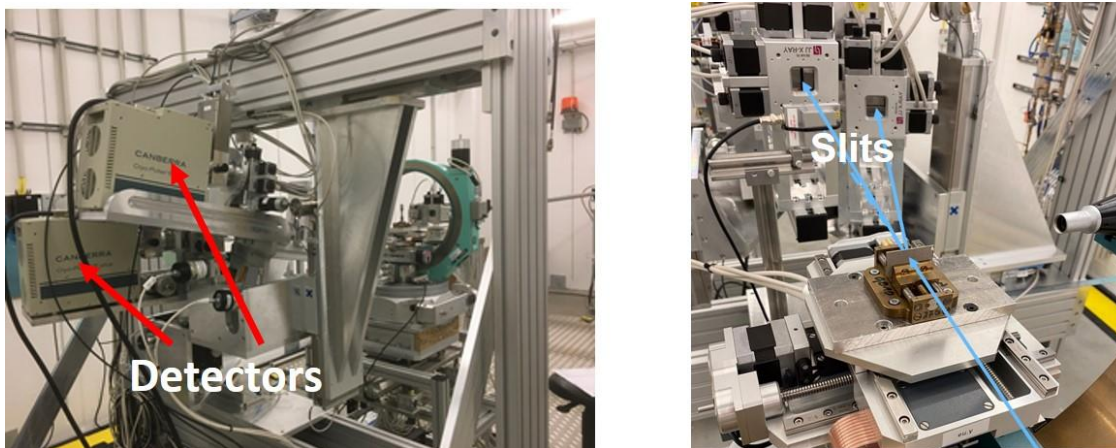
Figure 23 - Two Ge-detectors (left) with collimator slit system (right).

Table 7 - High purity Ge-detector specifications

Type	HP Ge-detector
FWHM 20 keV 122 keV	 160 eV 500 eV
Count rate	30% saturation at 10^6 cps
2θ range	-12° … 12° (hor); -12° … 12° (ver)
Aperture	max. 5×5 mm^2
Typical collection time	1 – 10 s* *estimated for most experiments. Must be increased for small incident beam applications
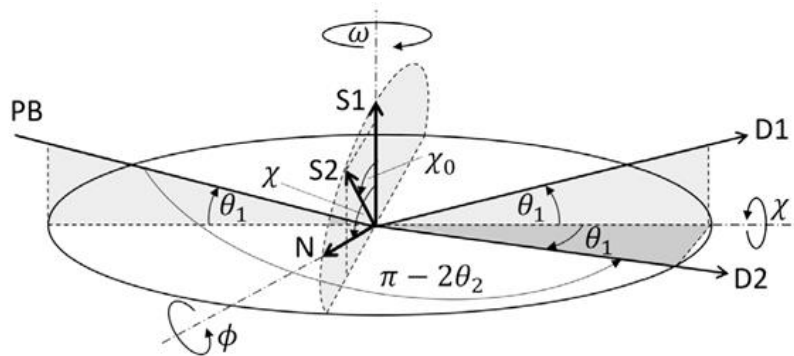
Figure 24 - Eulerian cradle nomenclature as stated in (Apel, 2018).

- Sample alignment: via the transmitted intensity collected by the beam stop photodiode current (Pico3). Si standard is used as calibration powder.
- Software: The beamline is fully integrated into the PETRA III experimental control, data transfer, and storage system. Motors in all experimental hutches are labelled with numbers as required for the Tango software tool kit and controlled by Python or Spock. TANGO is an object-oriented distributed control system, which is used at PETRA III for hardware control of most beamline components. Experimental data can be accessed remotely via the Gamma-Portal. Data-reduction and data analysis are performed with the in-house software P61A::Viewer and P61A::toolkit, respectively.

4.1.3. P07 High-Energy Materials Science Beamline at DESY - Hereon

The High Energy Materials Science Beamline (HEMS) P07 at PETRA III uses a monochromatic beam. It satisfies high-energy X-ray diffraction (XRD) and imaging techniques. The photon energy is tunable in the range 30 to 200 keV, and it is optimized for micrometric focusing with Compound Refractive Lenses (CRLs).

The materials and general science activities include a) fundamental research (metallurgy, chemistry, biology, etc), b) applied research for manufacturing process optimization, and c) experiments targeting the industrial user community which include environments for strain mapping on large structural components. Measurements at P07 include both depth-resolved residual stress analysis, i.e. with conical slits, and measurements in transmission geometry.

Experimental hutch (EH) EH3 (Fig. 25) is available, among many options, for strain scanning, and experimental hutch EH4 allows 3D-XRD grain mapping. EH1 is a side station that serves for feasibility tests, detector testing, education of students, and in-house research. EH2 is operated by DESY.
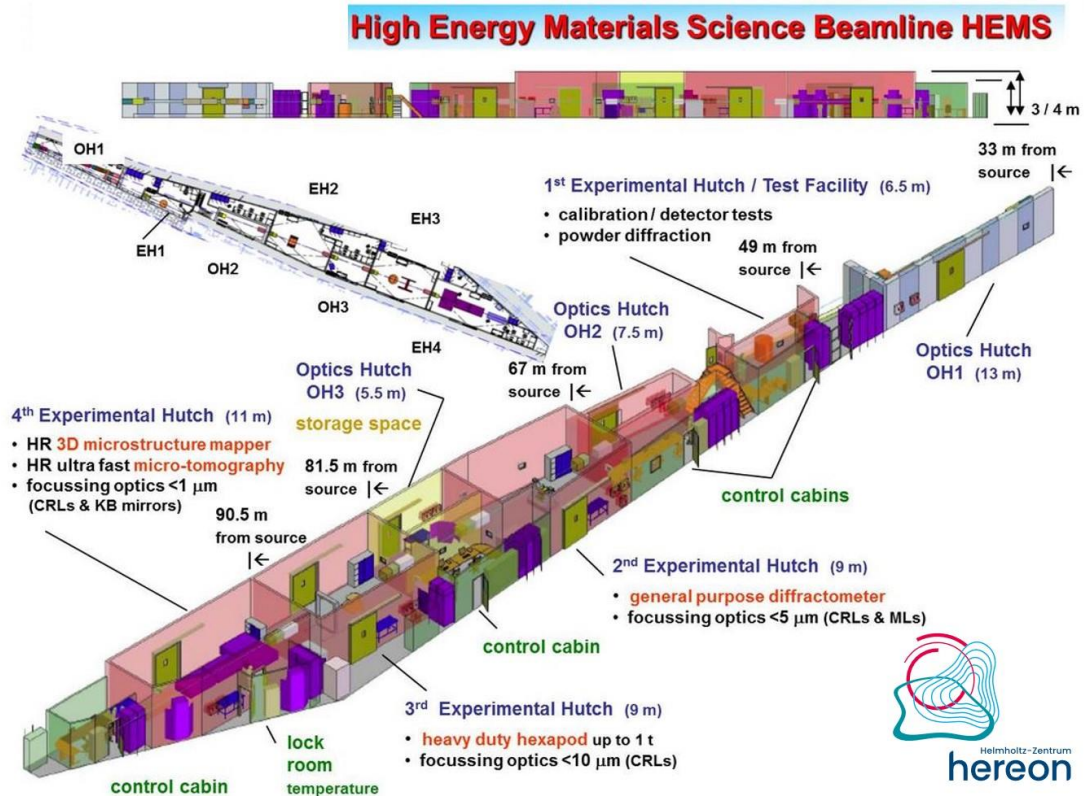
Figure 25 - Layout of the P07 HEMS beamline.

The main components of the instrument are:

- Optics: For EH3 (P07(a)), i.e. the main beam, the optics consist of two bent Si (111) Laue crystals (the first one water-cooled) on Rowland geometry (35.36° asymmetric cut, triangularly shaped with base 35 mm, length 89 mm and each 1.25 mm thick) in fixed exit (horizontal deviation 21 mm) keeping the beam at 1400 mm height above the floor. The energy is tuneable between ~ 30–200 keV with this double crystal monochromator (DCM) in horizontal scattering geometry (see Fig. 26). At 80 keV the sub-mm large beam showed an integrated flux of 5×10^{12} photons / sec. 0.2% bw. The maximum beam size is 1×1 mm^2. The optics for the side station EH1 [P07, a] consist of two flat water-cooled Laue crystals Si (111) and Si (220), 15 mm (wide) × 30 mm (high) × 1.5 mm (thick) on a lateral slide, with asymmetric angle 35.36°. The energy with this single bounce monochromator (SBM) can thus be switched between 53.7 keV and 87.1 keV (monochromator scattering angle fixed to horizontally 4.25°). The maximum beam size is 0.8×0.8 mm^2 with an integrated flux of approximately 5×10^{10} photons / sec. 0.01% bw at 87.1 keV.
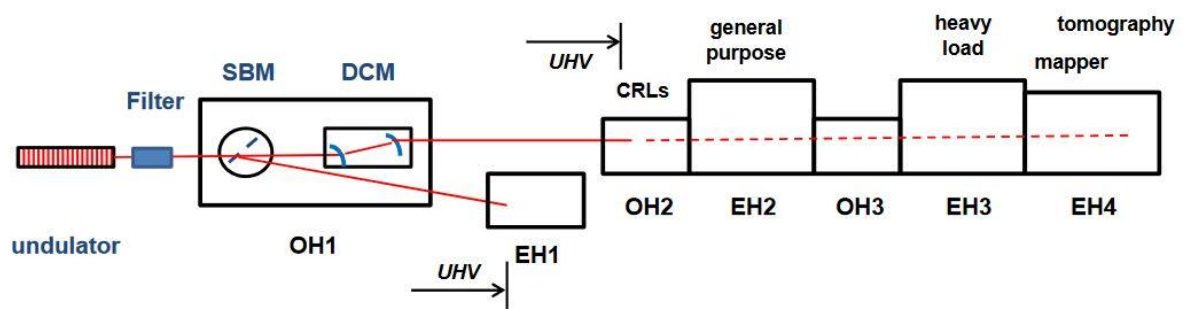
Figure 26 - Optics scheme in top view of the P07 HEMS beamline.

- X-ray source: the X-rays are produced by an IVU21 in-vacuum undulator (4.5 m long, 7 mm minimum gap).
- Instrumentation: the experimental hutch EH3 (Fig. 27) has a custom-built hexapod for heavy loads up to 1 t with positioning resolution of +/− 1 μm (travel ranges tens of cm, tilt angles 15°, Tab. 8). This hexapod provides the spatial sample movements in x, y, and z directions (Fig. 26) and a separate table allows rotations of +/− 180°. Conical slit cells (CSC) can be used for defining a gauge volume fixed in space. A small hexapod allows the alignment of the CSC. CSC (Fig. 29) can be used in both hutches, EH1 and EH3, requiring customized slit radii for their use with materials exhibiting BCC, FCC, and HCP lattices. The focal distance, i.e. the distance between the conical slit and the centre of the gauge volume, is 100 mm. For the experimental hutch EH1, the instrumentation is composed of a stage, which permits sample movement in x, y, and z directions (see Fig. 28). Additionally, a stage can be added for sample rotation around z axis which facilitates the sample alignment in the x-y plane. Sample oscillation is also enabled in x or z directions to increase statistics during the measurements. A mini-hexapod is used for the conical slit adjustment (fully orthogonal to the beam and with the beam passing through its centre). An additional set-up option is a closed Eulerian cradle on the goniometer stage.

Figure 27 - P07 - EH3 with JJ X-ray slits, big hexapod, conical slit cell set-up and PE detector on the detector portal.

Table 8 - Heavy-load hexapod specifications (P07(b)).

	PI Hexapod with load capacity 1 t and 1 μm resolution
Heavy Load Hexapod in EH3	Ranges: x: +202 / −237 mm; y: +/− 204 mm; z: +/− 100 mm u-Rx, v-Ry: +/− 20°; w-Rz: +/− 5° separate w-Rz rotation-table: +/− 180°
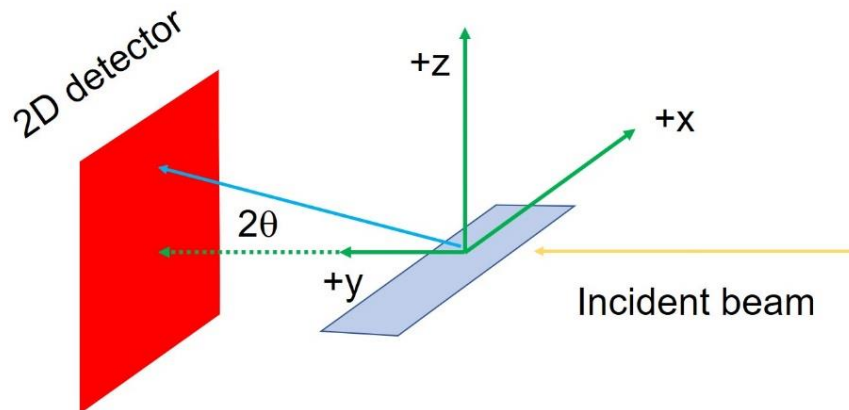
Figure 28 - Spatial directions at P07 in both EH1 and EH3 hutches.
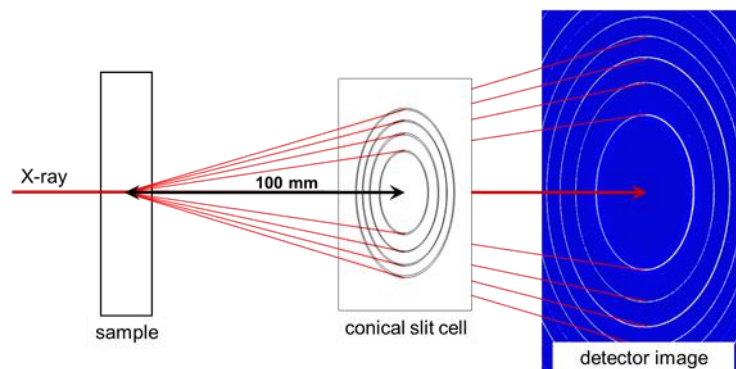
Figure 29 - Sketch of the conical slit cell setup.

- Detectors: for both hutches, EH1 and EH3, an in-house built detector portal allows the use of various 2D-detectors (P07(c)) (PE XRD 1621, mar345 image plate, PILATUS3 X CdTe 2M). Most commonly used are the PE detectors with an array of 2048×2048 pixels and pixel size of 200 μm. A new Varex detector XRD 4343RF (2880×2880 pixels and pixel size of 150 μm) is also available.
- Sample alignment: via the transmitted intensity collected by a photodiode. LaB$_6$ standard powders are used for instrumental calibration.
- Software: identically to the beamline P61A, P07 is fully integrated into the PETRA III experimental control, data transfer, and storage system. The Tango-based software is controlled by Online. The experimental data can also be accessed remotely via the Gamma-Portal. Fit2D is typically used for data reduction and analysis at the beamline.

4.1.4. ID22 2D diffraction setup with monochromatic beam at ESRF

At ESRF multiple beamlines (ID11, ID15a, ID22, ID31) may be used for strain scanning using a monochromatic beam and 2D detector. However, ID22 is the most used beamline for this purpose, due to the advantages of its configuration listed in the following. At the time of writing this document the development of a conical slit system is under discussion and could be available in the future. Also, measurements can be carried out in transmission on thin samples without the need of gauge volume definition. ID22 is a high-resolution powder diffraction beamline and residual strain/stress can be investigated using the traditional $\sin^2\psi$ method, in which the 2θ position of a diffraction peak is monitored in reflection geometry at different sample orientations (ψ). Such an approach can be used with soft X-rays, to give sensitivity to strain in the surface layers of a sample. Alternatively, with X-rays of energies up to 75 keV on ID22, measurements in transmission are possible. A gauge volume in the sample (from which the diffracted X-rays emanate) can be defined via slits and the analyser crystal (Fig. 30). A map of residual strain can be built up by translating the sample parallel and perpendicular to the beam and measuring the 2θ position of a peak for the different sample positions.
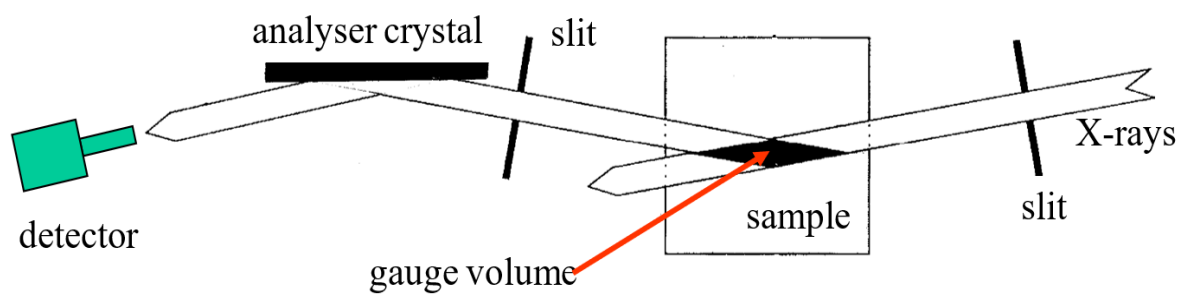
Figure 30 - Configuration for strain mapping using hard X-rays; the gauge volume has the cross section of a lozenge and is defined by the intersection of the incident and diffracted beams, defined by the combination of slits and the analyser crystal.

There are several advantages in using synchrotron X-rays and a high-resolution powder diffractometer equipped with an analyser crystal:

- The intrinsically narrow peak widths give enhanced sensitivity to shifts in peak positions.
- The peak widths are independent of ψ, unlike with the traditional Bragg-Brentano geometry, where loss of parafocusing leads to peak broadening.
- The wavelength tunability gives versatility. Soft X-rays can be selected for surface sensitivity. The depth of penetration can be varied by changing wavelength, even exploiting absorption edges, if appropriate. Hard X-rays ($\lambda \leq 0.3$ Å) allow transmission measurements and strain mapping.
- The use of an analyser crystal leads to accurate measurements free from the effects of surface shape or roughness, and confers immunity to aberrations that lead to undesired shifts in peak positions with conventional instruments, e.g. resulting from movement of the sample from the diffractometer axis, or surface effects (pseudostrains), when the gauge volume is only partially immersed in the sample. Thus, components with complex shapes are readily investigated.

The main components, but not limited to those cited, are:

- X-ray source: the X-rays are produced by an U26 in-vacuum undulator (2.5 m long, 6 mm minimum gap). It can cover the entire energy range from 6 keV to 80 keV (2.07 Å. to 0.15 Å in wavelength) with very high photon flux on both the soft- and hard-energy sides (ID22).

- Monochromator: the beam is monochromated by a channel cut Si (111) monochromator, with an overall length of 300 mm and a distance of 4 mm between the two diffracting surfaces. The second surface can be tuned to compensate for changes in the Bragg angle caused by changes in the heat load. The first block of the monochromator crystal, which has the highest heat load, is side cooled to about 105 K by copper blocks through which liquid nitrogen flows. Water-cooled slits define the size of the beam incident on the monochromator, and of the monochromatic beam transmitted to the sample, typically in the range 0.5–1.6 mm (horizontal) by 0.1–1.5 mm (vertical) (ID22).

- Transfocator: for strain-mapping experiments, the beam will be focussed to 50 μm to improve spatial resolution and efficiency, instead of cutting down the beam with slits. Strain scanning will also benefit from the enhanced hard-energy performance, permitting the investigation of thicker components and those made of highly absorbing materials such as steel and nickel. It will also be possible to combine a focussed beam of energy 80 keV with an area detector.

- Sample stage: the sample stage installed at ID22 can support up to 20 kg of load. The strokes of the motors used to map the sample are given in Tab. 9.

- Multianalyzer stage: ID22 is equipped with thirteen Si (111) analyser crystals mounted on a single rotation stage. The multi-analyser crystal stage is positioned before the detector and is intercepting the diffracted beam. To be recorded by the detector the diffracted beam must strike the analyser crystal at precisely the correct Bragg angle. Since the acceptance of an Si (111) crystal is very small (a few arcseconds), it stringently defines the 2θ angle of diffraction yielding very narrow diffraction peaks (Dejoie, 2018). Given also the mechanical integrity and angular accuracy of the diffractometer installed at ID22, the peak positions are accurate and reproducible to a few tenths of a millidegree. The multi-analyser stage allows to attain a high-resolution giving a high sensitivity to the peak shift. The use of an analyser crystal leads to accurate measurements free from the effects of surface shape or roughness, and confers immunity to aberrations that lead to undesired shifts in peak positions with conventional instruments, e.g. resulting from movement of the sample from the diffractometer axis, or surface effects (pseudo strains), when the gauge volume is only partially immersed in the sample. Therefore, a high strain resolution can be obtained.

- 2D detector: the flat panel Perkin Elmer XRD 1611CP3 is available. The XRD 1611 consists of a 41×41 cm^2 CsI scintillator bonded to an amorphous silicon substrate. The detector has a pixel size of 100×100 μm^2 and potentially a maximum readout speed of 3.75 frames per second (fps) at maximum resolution. Installed on a motorized linear translation stage that allows variation of the sample-detector distance between 380 and 2500 mm, it can be used to attain a maximum momentum transfer in one shot (Q_{max}) of up to 25 Å^{-1} at 80 keV). The acquisition workstation is based on the "LIMA" software library developed by ESRF for 2D detector control and data acquisition. On-the-fly dark-current image subtraction is possible to correct for the heterogeneity in the pixel response to photons and afterglow. 2D powder diffraction data reduction software is available for calibration and data integration.

Table 9 - Motor stroke and resolution of the sample stage.

Motor	Travel	Resolution
T_x	80 mm	0.001 mm
T_y	80 mm	0.001 mm
T_z	100 mm	0.01 mm

4.2. Neutron techniques

4.2.1. SALSA – Strain Analyser for Large Scaled engineering Application at ILL (Grenoble)

SALSA (Stress Analyzer for Large Scaled engineering Applications) is one of the suites of forty-seven instruments of the Institut Max von Laue - Paul Langevin (ILL) in Grenoble, France. The ILL operates a high flux nuclear fission reactor, providing neutron beams to 47 scientific instruments for peaceful research. SALSA is a monochromatic two-axis neutron strain scanner optimised for residual stress analysis of engineering components (Pirling, 2006) and was built in the framework of the ILL Millennium Program and co-funded by the U.K. Engineering and Physical Sciences Research Council (EPSRC). It started operation in 2005, replacing the high-resolution powder diffractometer D1A, which was partially used for stress determination before. SALSA is installed on a super-mirror neutron guide, internal designation H22, with a relative critical angle of total reflection of m = 2. The super-mirror guide delivers high neutron flux, while the instrument's location in a guide hall ensures low background. A photo of the actual set up and the schematic of the main components of the instrument are provided in Fig. 31. A detailed overview of components from the top and also in 3D is provided in Fig. 32 and each component is detailed in the following subsections.
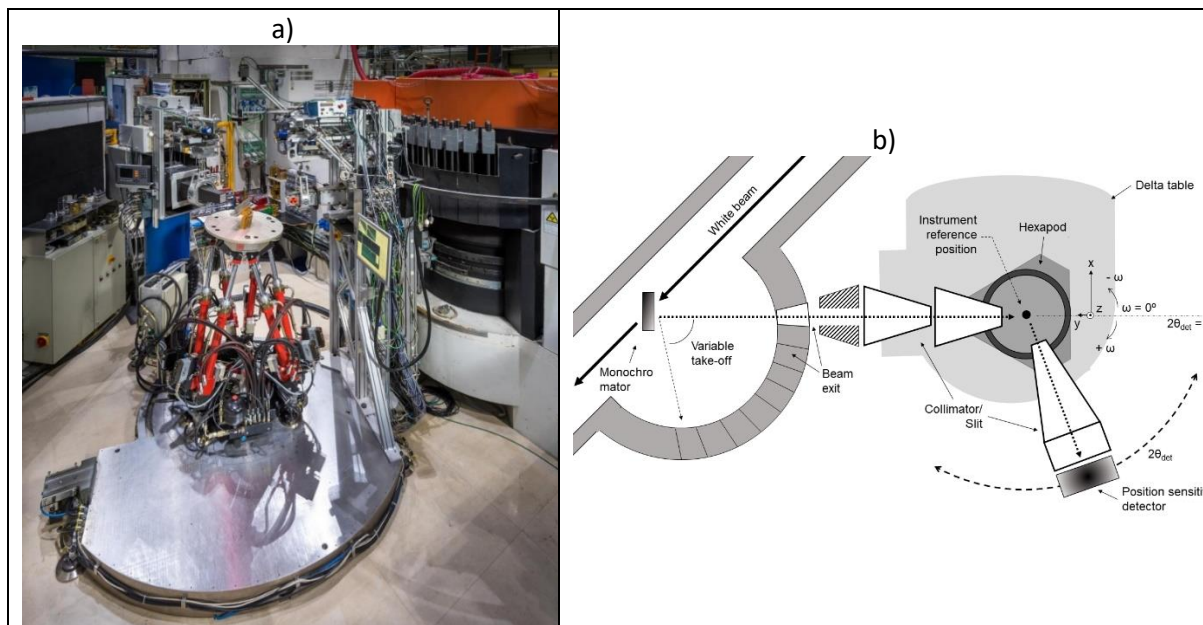
Figure 31 - SALSA strain diffractometer set-up at ILL a) actual front photo b) top view scheme of components.
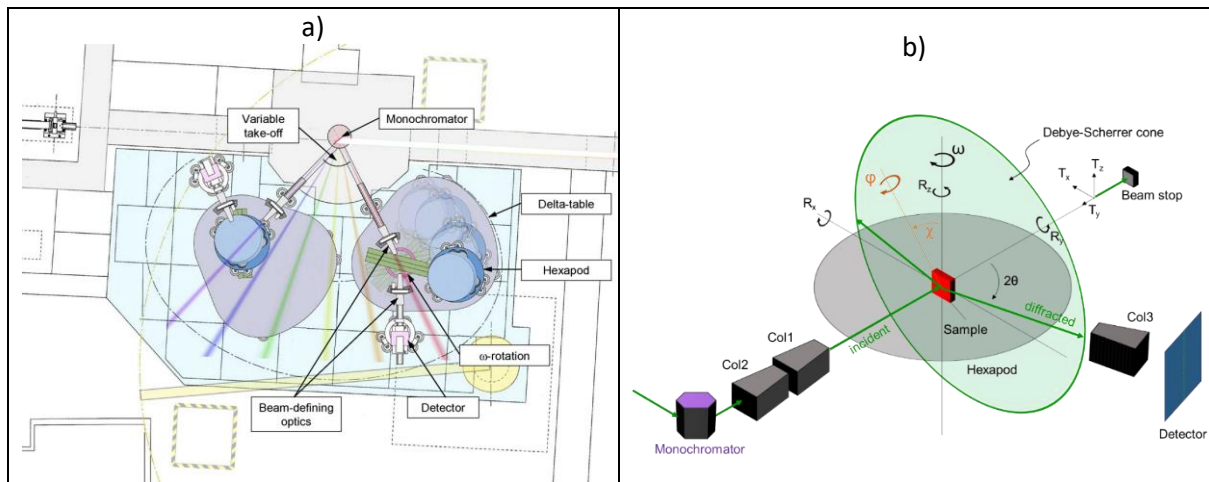
Figure 32 - a) Schematics of SALSA beamline showing its position at minimum and maximum take-off angle, b) beam path. Col1 – Col3: radial focussing collimators for gauge volume definition.

The main components of the SALSA instrument, summarized in Tab. 10 and Tab. 11, are:

- Delta table: The so-called delta-table of 2.5 m^2 size connects all components of the secondary diffractometer. It is the base for primary optics, contains the omega rotation bearing, which is linked to the hexapod and the guidance for the detector support with secondary optics. It allows the change of the take-off angle for wavelength selection without changing the measuring geometry. For this purpose, it is linked to a rotation bearing, which is well aligned with the monochromator omega-axis.

- Monochromator: Inside the casemate and aligned with the beam guide exit, a carrousel table permits to host up to three monochromators. At the moment there are two in place: Ge from D1A (not in use) and a Si one. A copper monochromator has recently been approved for installation in 2023, enhancing better flux at wavelengths above 2 Å. The SALSA Si monochromator (Fig. 33) is a variable bending double-focusing type with 39 Si perfect crystal panels of 12 mm × 165 mm × 5 mm size. Its design provides the advantage of increased neutron flux at the sample position due to a lateral condensation of the beam in vertical direction and higher angular resolution due to focusing in momentum space in the diffraction plane. In combination with radial focusing collimators, the configuration aims at maximising the flux at the sample position, while achieving optimum lateral and angular resolution. The neutron flux at the sample position is in the range of 10^7 n cm^{-2} s^{-1}. The Si monochromator provides a wavelength range of 1.5-2.4 Å. The particular [1 0 0] crystal cut, which is optimised to provide λ = 1.66 Å using the Si (4 0 0) reflection, is ideal for most engineering metal applications (Fe, Al, Ni, Cu alloys, etc.) in a 2ϑ near 90° configuration allowing the definition of a cubic gauge volume. The wavelength can be changed continuously by altering the take-off angle (Fig. 32) and by choosing one of the monochromator reflections Si (400), Si (422), Si (511) or Si (311). Focalisation in phase space is achieved by adjusting the curvature of the monochromator crystals. It can be optimised for maximum intensity, best strain resolution or best overall performance, maximising a figure of merit. In any case its optimisation is only valid within a limited 2Ɵ range of about ± 5°. In other words, it must be optimised for the Bragg-reflection of the sample material used for measurements.
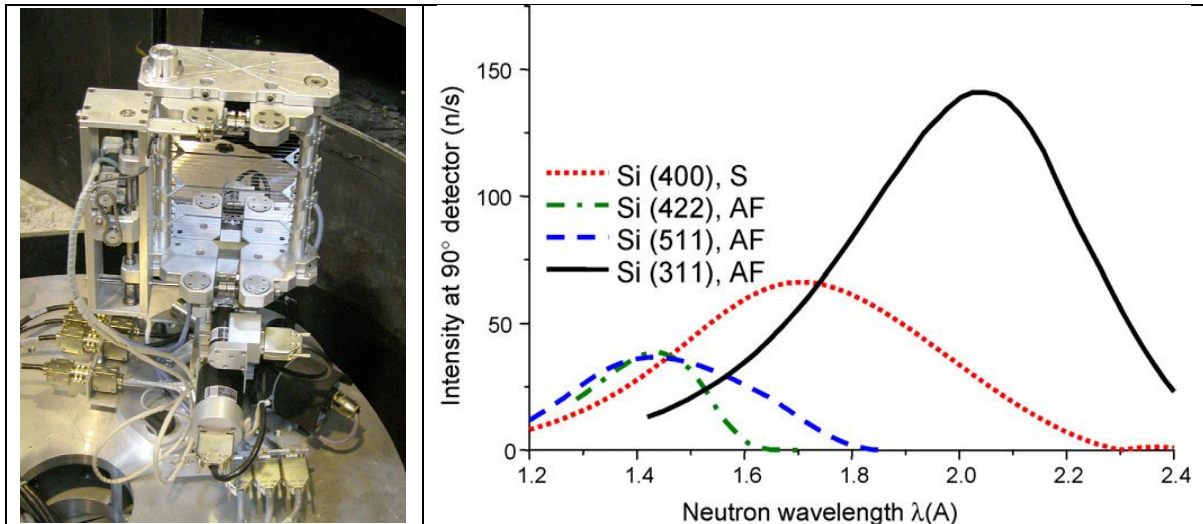
Figure 33 - Si- double bending monochromator and relationship between intensity and wavelength (considering optimum take-off for each curve).

- Beam optics: Radial collimators and/or slits can be used for gauge volume definition, both on the primary (incident) beam and the secondary (diffracted) beam sides. The suite of radial collimators on SALSA provide options to define beam sizes with full-width-at-half-maximum of either 0.6 mm, 2 mm or 4 mm respectively (horizontal and vertical, arranged in series) for both the primary and secondary beam. Their advantages are the transmission of the full divergence of the focussed beam from the monochromator and at the same time defining a precise focus. Their focal distances (between 150 mm and 411 mm) leave space for large samples and sample-movements. On the secondary side, the collimators image the full diffraction peak without distortions such as clipping effects that occur with slit optics. As a result, strain gradients are imaged correctly and pseudo peak shifts as they arise in measurements near surfaces or interfaces are drastically reduced and can be corrected. It is possible to determine strain gradients typically from 100 μm on and in microstructurally appropriate cases even from 40 μm on. This type of measurements is nowadays common practice on SALSA. For more flexible gauge volume dimensions, automated slit systems may be used instead.
- Different sample stages and cradles are available:
  - Hexapod: parallel kinematic steward platform with six degrees of freedom achieved by using six independent hydraulically controlled pistons. The hexapod slides on air-pads on the delta table is linked to the omega rotation bearing, allowing 360° rotation and can be displaced away from the omega-axis by up to 700 mm thanks to a 7th hydraulic cylinder. This feature allows mounting very large samples centred on the hexapod, but measured at an extremity or helps installing large sample environment before bringing it to the measuring position. The construction is compact, light, yet very stiff and therefore ideal for accurate manipulation of heavy samples. It enables sample support of over 900 kg, with a range of motion of ±300 mm translation in *x* and *y*, 150 mm in *z*, and tilt range of ±30° (without considering the horizontal piston movement). A main advantage of the hexapod sample stage for strain scanning is the possibility of tilt and translation at the same time. This allows efficient and precise orientation of complex shaped, and even large samples, with respect to the neutron beam.

- Omega table: the hexapod sits on the 360° omega-rotation table allowing for horizontal **Q** (scattering vector) orientation in the sample with a single set up and alignment.
- Cradle: A ¼ circle Eulerian cradle and a compact rotation stage are also available to mount on top of the hexapod to provide an extra angular motion for sample orientation vs. scattering vector *Q* (i.e., strain component).
- Rotation stage: positioning or continuous rotation of samples of up to 50 kg weight.
- Detector: Neutron detection is carried out by a 2-D position sensitive 3He detector (PSD) with an active area of 250 x 250 mm2, covering 11° in 2θ. It consists of 2 x 128 wires at 2 mm spacing. By interpolation it provides 256 × 256 pixels, which translates in a channel width of 0.044°.
- Hardware (HW) and software (SW) used during the measurements are listed in the following:
  - Acquisition card: Two general modes are available: time or count dependent acquisition and event mode with 2 digital, 1 incremental encoder and 4 analogue channels.
  - NOMAD: instrument control
  - VISA: allows remote access to the instrument and analysis software.
  - Data reduction: Large Array Manipulation Program (LAMP) software developed at ILL.
  - Data analysis: Strain/stress calculations as well as pseudo-strain correction from entry scans are performed using in-house developed MathCad-based codes (PS-FIT, Pirling, personal communication, 2019), and a Phyton-based routine (Cabrera and Cabeza, personal communication, 2019).

Table 10 - Technical specification of SALSA strain diffractometer.

SALSA	
Type	Two-Axes Strain Diffractometer
Monochromator/ Moderator Take-off angle [°]	Bent Si(400), (422), (511), (311), 55 -125
Wavelength [Å]	1.3 – 3 (monochromatic)
Beam optics [mm]	Primary radial collimators: 0.6&2&4 mm (vert.&hor.); 10 mm (vert), aperture 20 mm (vert).; Secondary radial collimators: 0.6&2&4 mm (hor),
Sample positioning system (SPS)	Hexapod, max. load 1000 kg, *xy*-range ±300 mm, *z*-range 150 mm, tilt & rotation, ¼ cradle
SPS accuracy	±5 µm for > 500 kg sample
Detector	PSD 250 × 250 mm^2, 256 × 256 pixel, 0.044° × 0.044°
Sample alignment	Telecentric cameras + CMM touch & laser probe

Table 11 - Technical specification of the different SALSA components.

Monochromator	
Wavelength-range:	1.3-3 Å
Continuously, variable take-off	55° - 125°
Δd/d	Typ. 0.3%
Flux at sample position (at 1.6 Å)	$2 \cdot 10^7 \text{ cm}^{-2}\text{s}^{-1}$
Beam shaping optics	
Slit apertures, continuously variable	0.1 – 5 mm
Radial collimators	0.6 / 2 / 4 / 10 mm
Detector	
Type	^{3}He, 2dim Position Sensitive wire
Range / resolution	11°, 128 wires, 0.045°/channel
Hexapod sample stage	
Tilt	+/- 11° - max +/- 30°
Translation: x / y / z	(600 / 600 + 700 mm / 340) mm
Positioning accuracy	5 mm
Sample dimensions	0.5 mm – 1.5 m
Load capacity	max. 1000 kg
Eulerian-cradle	
Angular range	90°
Radius	245 mm
Load	50 kg
Alignment	
Camera assisted metrology system	21 mm
VAMAS sample mount	
NQL calibration tower	Fe-, Cu- and Ni- foils Feritic steel pins 1-3-5 mm diameter
Software	
Control Software	NOMAD
Remote access	VISA

Acquisition modes:	counts, time, kinetic, event mode
Data-reduction:	LAMP, SteCa
Data analysis	Mathcad, Python, Excel, Origin

4.2.2. ATHOS - Neutron diffractometer for strain analysis at BNC

ATHOS (in Fig. 20) is one of the 11 instruments of the Budapest Neutron Centre (BNC) at the Budapest Research Reactor. BNC is a group of departments of the Centre for Energy Research. ATHOS was originally a three axis spectrometer (TAS) for studying medium – low energy excitations on single crystal sample, but at the beginning of the last development period it was decided to develop and optimize for strain measurement. ATHOS is situated at the cold neutron beamline No. 1 in the cold neutron hall of BNC. The beamline starts at the liquid H filled cold neutron source which gives a spectrum with the peak at 2.5 A. The beam is lead from the source to the instrument using a neutron guide.
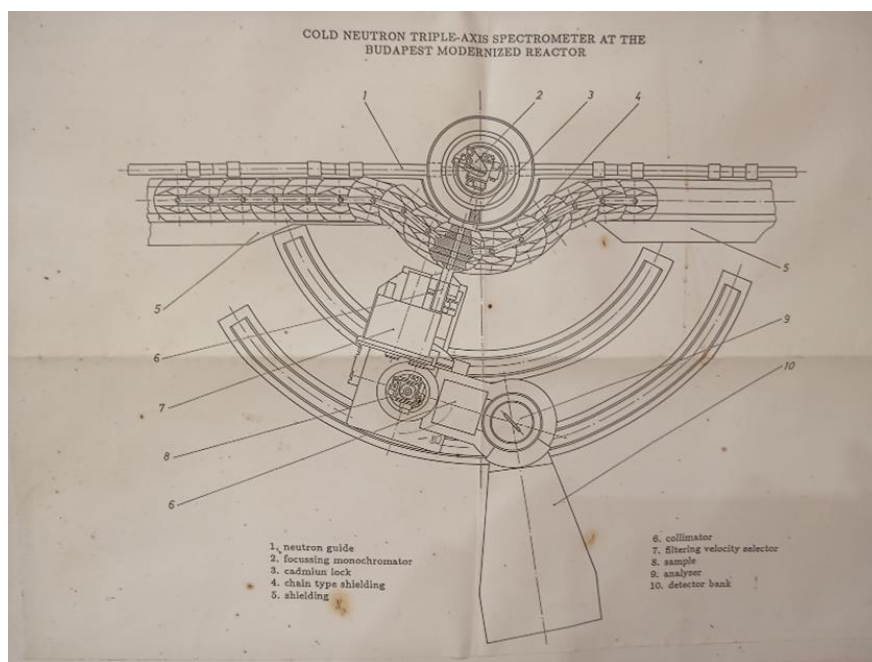
Figure 34 - Drawing of ATHOS in TAS mode.

The main components of ATHOS, reported also in Tab. 12 and Tab. 13, are:

- Neutron guide: consisting of neutron supermirrors with the coating of $m = 2$ giving the critical reflection angle of 0.5° at 2.5 Å. The neutron guide has the width of 25 mm and the height of 100 mm. The wall between the reactor hall and the cold hall together with the extra borated paraffin and concrete shielding within the biological shielding gives low background conditions but since the instrument is close to the reactor, and the guide cannot go out of line of sight some fast neutron can go through the neutron guide. Downstream of ATHOS three other instruments are on the same beamline: neutron reflectometer and prompt gamma activation analyser (PGAA) and neutron induced prompt gamma spectrometer (NIPS) prompt

gamma activation analysis instruments. PGAA and NIPS cannot work at the same time. NIPS is equipped with a neutron camera making it able to make prompt gamma activation imaging experiments.

- Monochromator (Fig. 35) pyrolithic graphite, mosaicity is 0.4° FWHM for selecting the neutrons with a given wavelength. For monochromatization (002) and (004) reflections are used. The monochromator is vertically focused. Since the beam width at the monochromator is small (25 mm) and the monochromator – sample distance is large (2200 mm), horizontal focusing would not cause significant change neither on the intensity nor on the resolution. The monochromator can be adjusted using a goniometer integrated with an XY table, the degree of freedom is 5: moving in two perpendicular horizontal directions, tilting around to perpendicular horizontal axis and rotating around the vertical axis. The monochromator take-of angle and the monochromator scattering angle (angle between the beam direction in the neutron guide and the [002] lattice plane of the monochromator) are mechanically connected, apart from the vertical adjustment omega part of the goniometer the monochromator angle and the take-of angle moves in $\theta - 2\theta$ setting. Original sample table and the original 2θ arm was used for inelastic neutron scattering study. For strain measurement the original 2θ arm is set to the direction of the incident beam.
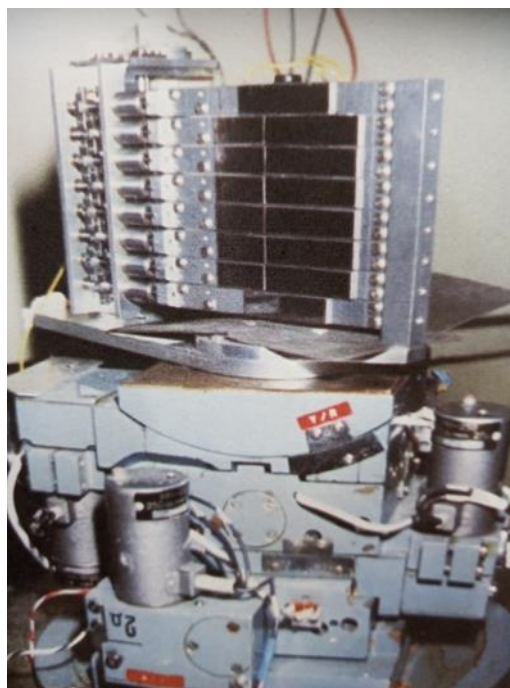
Figure 35 - Monochromator of ATHOS instrument.

- Sample table: the sample table was used for inelastic study as an analyser table, for strain measurement it is used as a sample table. It is equipped with an omega table with the diameter of 400 mm. The centre of the sample table is set to the centre of the beam reflected by the monochromator (by setting the original 2θ arm to 0°). A XY/(XZ)-table (Fig. 36) moves the sample in two horizontal direction or one horizontal and one vertical direction to set the point in the sample for the given strain measurement. The range of the movement is 100 mm for each direction. An XYZ table is designed (Fig. 36) to be able to move the sample in three

directions (four degree of freedom together with the omega table). The production of the XYZ table will start soon.
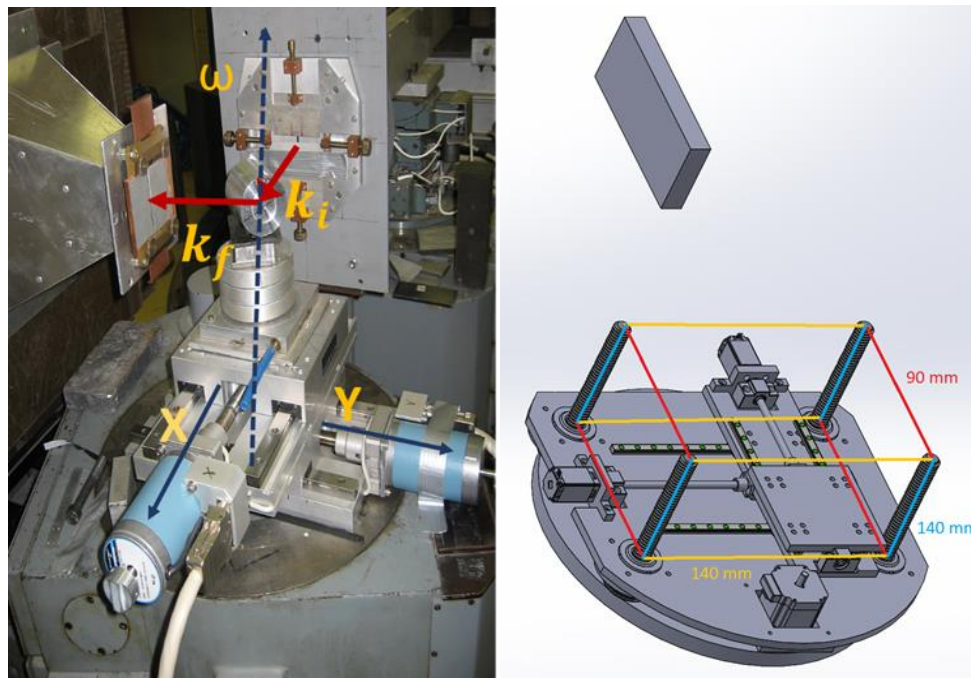
Figure 36 - Present and planned sample positioning system of ATHOS instrument left and right respectively.

- Slit system is used to form the beam, set the gauge volume size and shape, and position the gauge volume to the intersection of the incident beam and the vertical axis of the omega table. The slit system consists of three slits: one fixed aperture with the width of 25 mm and height of 100 mm is placed at the entry of the monochromator shielding. The aperture is used to reduce the background originated from the monochromator casemate. The pre-sample slit is adjustable vertically and horizontally. It sets the horizontal and vertical size of the incident beam i.e. it sets the height and the width (perpendicular to the incident beam) of the gauge volume. The pre-sample slit can be moved in the direction of the incident beam from 100 mm to 200 mm upstream from the centre of the gauge volume. The after-sample slit is situated between the detector and the sample. It is used to determine the horizontal size of the gauge volume perpendicular to the reflected beam. The after-sample slit can be adjusted in vertical and horizontal direction. In the horizontal direction it defines the gauge volume, in vertical direction it is opened to enable to cover the detector by the reflected beam, i.e the goal of the vertical setting is to reduce the background originated outside of the sample. The after-sample slit can be moved together with the detector, the smallest distance from the sample is 100 mm. The absorbing material of the adjustable slits is cadmium, while that of the fix aperture is Mirrobor which is plastic with high boron carbide content (>80 mass %). The slits can be moved presently by hand. Replacing them with new, electronically adjustable slits is and integration of a radial collimator with the FWHM of the focal point of 3 mm is ongoing.
- Detector is a 2D ^{3}He filled proportional position sensitive detector with the resolution of 1.8 mm. The distance between the collector wires is 1 mm both for anode and cathode planes. The readout is delay – line type. The minimal sample – detector distance is 900 mm. The

detector is surrounded by 100 mm of plastic with medium boron content, at the side facing to the sample 5 mm Mirrobor is used inside a converging nose.

Table 12 - Technical specification of ATHOS strain diffractometer.

ATHOS	
Type	Two-Axes Strain Diffractometer / Three-Axis spectrometer
Monochromator/ Moderator Take-off angle [°]	Vertically focusing pyrolithic graphite (002), (004) 33 -126
Wavelength [Å]	2 – 6 and 1-3 (monochromatic) for (002) and (004) reflections respectively
Beam optics [mm]	Primary aperture: 25&100 mm (vert.&hor.); Pre-sample slit: 1-5&1-5 mm (vert.&hor.); After-sample slit: 1-5&1-25 mm (vert.&hor.);
Sample positioning system (SPS)	Omega-table max load 40 kg, XY / XZ table, range ±50 mm
SPS accuracy	±10 µm
Detector	PSD 250 × 250 mm^2, 256 × 256 pixel, 0.044° × 0.044°
Sample alignment	Telecentric cameras + CMM touch & laser probe

Table 13 - Technical specification of the different ATHOS components.

Monochromator	
Wavelength-range:	1-6 Å
Continuously, variable take-off	55° - 125°
Δd/d	Typ. 0.3%
Flux at sample position (at 1.6 Å)	$2 * 10^5$ cm^{-2}s^{-1}
Beam shaping optics	
Slit apertures, continuously variable	1 – 5 mm
Radial collimators	No
Detector	
Type	^{3}He, 2D proportional Position Sensitive wire chamber

Range / resolution	11°, 200 wires, 0.05°/channel, 1.8mm total resolution
Alignment	
Laser + theodolite	
NQL calibration	Feritic steel pin 3 mm diameter
Software	
Control Software	ZsaMo (python, own development)
Remote access	ZsaMo (python own development)
Acquisition modes:	counts, time
Data-reduction:	Datared (python,own development)
Data analysis	Datared (python,own development)

5. Operating procedures for diffraction techniques

In the following section are enlisted the operating procedures developed for each residual stress measurement technique.

5.1. Energy-dispersive X-ray diffraction - Transmission mode

5.1.1. Preparation for measurements in EDXRD Transmission mode

a. Detector calibration

The aim of the detector calibration is to determine the coefficients for the conversion from channels to energy. The determination of the coefficients for the conversion from channels to energy should be done using a well-known radioactive source. The used calibration source should cover the whole energy spectrum that will be used for the experiments. Extrapolation must be avoided in the conversion from channels to energy. The steps to be followed are:

1. The fluorescence lines of the radioactive source are acquired.
2. Secondly, their positions have to be determined.
3. The coefficients are determined by the fitting of a polynomial function defining the evolution of the energy as a function of the channels.

An example of the determination of the coefficients for the conversion from channels to energy is illustrated in Fig. 37.
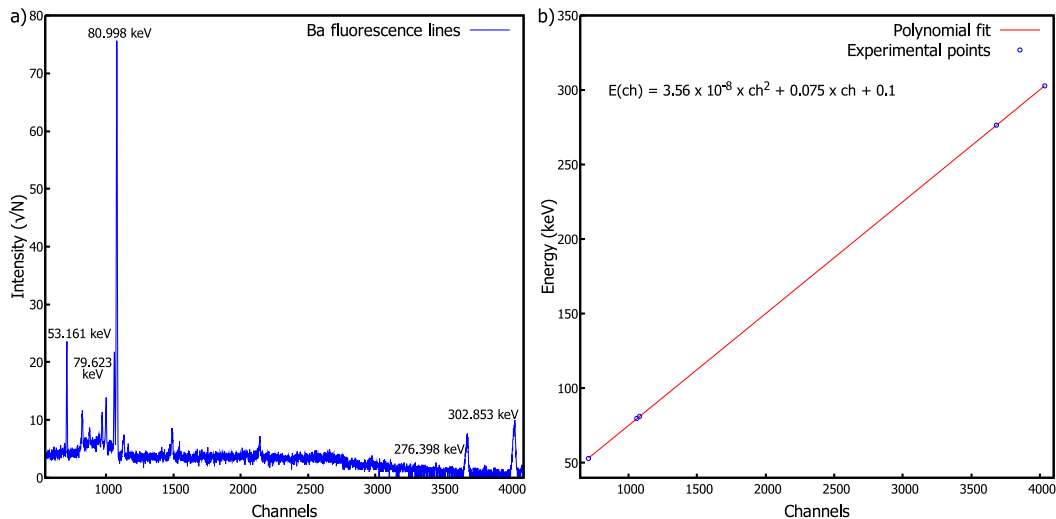
Figure 37 - a) Example of Ba radioactive source fluorescence lines and b) determination of the coefficients by polynomial fitting.

b. Alignment of the instrument

The alignment of the optics and the slits defining the incident beam have to be done. Then, the main goal of the instrument alignment is to ensure that the centroid of the gauge volume coincides with the centre of rotation of the sample stage or Eulerian cradle. The main steps of the procedure to align the instrument are:

1. Find the centre of rotation of the sample stage using a pin or another similar diffracting object, which will be used later to centre on it the gauge volume, i.e. the detectors and the slits defining the gauge volume.
2. Put the centre of the rotation of the sample stage on the beam.
3. Centre the slits and the detectors, i.e. the gauge volume, on the pin, i.e. the rotation centre of the sample stage.
4. Ensure that the used detectors are recording diffracted photons coming from the same volume in the sample.

To ensure that the detectors are looking to the same volume in the sample, a thin foil (thinner than the expected gauge volume length) should be scanned along the beam direction. The diffracted integrated intensity is plotted as function of the sample position. An example is shown in Fig. 38. The full width at half maximum (FWHM) of the curve of the intensity with respect to the sample position represents the length of the gauge volume. If the slit sizes defining the diffracted beam are the same, the curves of the two detectors should have the same centre and the same FWHM.
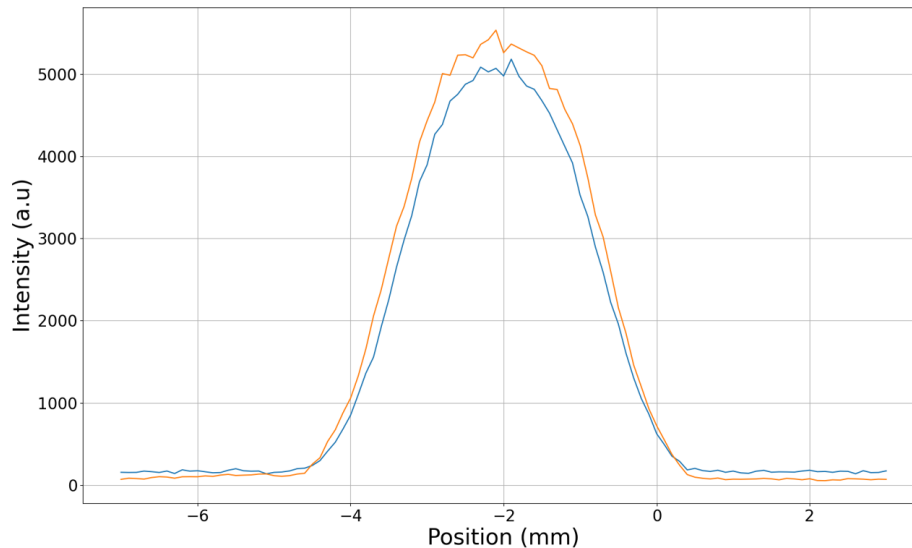
Figure 38 - Integral intensity recorded by the two detectors as function of the thin foil position along the beam. Orange: Horizontal detector, Blue: Vertical detector.

c. Calibration of the diffraction angle

The aim of the calibration of the diffraction angle is to determine precisely the diffraction angle at which the detector is fixed. It can be done using a well-known reference sample (strain-free sample). Knowing the lattice parameters of the reference sample, the diffraction angle can be determined using Eq. 15. As many as possible (hkl) reflections should be used for the calibration of the diffraction angle.

$$2\theta = 2 \times arcsin\left(\frac{h \times c}{2 \times d^{hkl} \times E^{hkl}}\right)$$

Eq. 15

with 2θ the diffraction angle, h the Planck's constant, c the velocity of light, d^{hkl} the theoretical lattice spacing of the reference sample and E^{hkl} the experimental energy of the family of (hkl) planes.

d. Gauge volume dimensions

The dimensions of the gauge volume should be measured and reported for each used detector.

e. Choice of the dimensions and the positioning of the gauge volume

The use of synchrotron high energy X-rays results in a small diffraction angle. Thus, the gauge volume is not homogeneous in all directions and has a diamond shape with an elongated dimension in the direction of the beam (see Fig. 8 and Fig. 10). Therefore, the dimensions of the gauge volume (GV) and its positioning within the sample should be optimized. For example, it is preferable to avoid to place the length of the gauge volume in the direction of the strain/stress gradient. The volume of the GV must allow the sampling of a representative volume within the sample, i.e. illuminate a sufficient

number of grains within the sample. To avoid energy drift, the gauge volume should be fully immerged within the sample.

f. Sample positioning

A reference in the sample must be defined and adopted for the measurements and data processing. The surfaces of the sample or fiducial marks should be determined relative to the centre of the gauge volume. The position of the centre of the gauge volume must be known in relation to the reference point in the sample. The finding of the surfaces and the positioning of the centre of the gauge volume could be done using optic/camera or mechanic system, if available at the beamline or using X-rays via repeated scans through the surfaces and edges of the sample. A particular attention has to be taken on the alignment of the sample relative to the beam and the gauge volume.

5.1.2. Measurement and recording requirements

a. General

From the measurements, the following quantities should be aimed to be extracted:

- The strain at different directions.
- The direction of each measured strain in the sample reference.
- The position (coordinates), in the sample reference, of the point at which the strain was measured.
- The dimensions of the used gauge volume.

b. Required information

From the data acquisition step, several information containing data and metadata shall be reported. A list of parameters is given in Tab. 14.

Table 14 - Metadata and data to be recorded during measurement (this is not an exhaustive list).

Metadata	Data
- Name of the facility - Source type (Synchrotron, Neutrons, …) - Name of the instrument/beamline - Name of the proposal - DOI identifier - Name of the sample - Start and end time - Beam mode (Monochromatic, white, …) - Filling mode - Detector(s) type - Type of acquisition - Sketch explaining the setup, the different references and sample	- Data recorded by all the counters (ex: photodiode, monitor, current, …) - Data recorded by all the detectors - Data needed to qualify the quality of the measurement (ex: count rate, events, dead time, …) - Positions of all the motors (ex: position in the instrument reference, monochromator, undulator, energy, …) - Acquisition time - Dimensions of the gauge volume

| positioning in relation to the instrument reference (might be a picture, drawing, notes, logbook, …) | |

c. Specimen coordinates

The coordinate system should be clearly defined. The chosen reference shall relate to the shape of the specimen and/or to the principal stress directions, if known.

d. Measurement directions

For a complete strain/stress tensor determination of at least six independent measurement directions should be probed. The choice of the measurement direction is dependent on the aim of the measurement (strain/stress aimed for the measurement). If the principal stress directions are known beforehand, strain measurements in the principal directions are sufficient to calculate the principal stress components. The measurement directions should be clearly defined in the sample reference for each measurement point (acquisition).

When orientating the sample, a particular attention should be given to the volume occupied in the material by the gauge volume. When rotating the sample, the gauge volume occupies different volumes in the material due to its diamond/lozenge shape. Therefore, different volumes are sampled.

e. Measured strain

The measured strain represents an average of all the strains measured from the volume of material occupied by the gauge volume. The strain values should be reported to the position of the centroid of the gauge volume in the material. To avoid pseudo-strain effect, the gauge volume should be entirely filled. If the gauge volume is not fully immerged in the material, pseudo-strain correction should be done.

f. Detector electronics effects

The detector performance in term of energy resolution and stability and their dependence to the electronic signal processing parameters, dead time and count rate must be known. More information on the influence of the detector electronic effects on residual stress measurement can be found in the literature (Denks, 2007) (Honkimaki, 2007) (Apel M. K., 2014).

5.2. Energy-dispersive X-ray diffraction - Reflection mode

5.2.1. Preparation for measurements in EDXRD Reflection mode

a. Instrument setup

Steps a, b, and c from section 5.1.1 should be done.

b. Measurement parameter selection

The measurement parameters should be identified to address the measurement requirements:

- The diffraction angle should be chosen according to the desired depth investigated
- The range for ψ and ϕ scanning, as well as the number of steps should be chosen
- Test measurements should be done to identify if any diffraction peaks overlap with fluorescence lines.

c. Sample positioning

The surfaces to be measured should be identified and located in the cradle coordinate system. This can be done through optical alignment (cameras, alignment lasers, etc.) or by using the incident beam to identify features in the sample, such as edges or pre-placed markers. Energy dispersive reflection measurements are particularly sensitive to surface height misalignment, which leads to pseudo stresses on $\sin^2\psi$ scans. The surface point to be measured must be positioned in the centre of rotation of the cradle within 50 μm resolution. Particular attention must be given to samples with rough surface finish or samples with a convex surface shape. In such cases, a local height measurement with a laser interferometer, micrometre or the beam gauge volume itself is recommended. The beam angle of incidence on the surface is typically taken as $2\theta/2$.

d. Slit positioning

On reflection measurements, it is important to guarantee that photons can arrive at the detector departing from a wide range of depths. This means that slits should not be closed enough to introduce a bias on the observed depth range. Ideal measurements are obtained with a large incident beam and narrow diffracted beam sizes. Since divergence at synchrotron sources is typically small, a large incident beam does not affect the incident beam divergence, whereas on the detector collimating slits, a small variation in beam size can lead to a large increase in divergence. As a reference, at P61A reflection experiments are typically done with 0.5 x 0.5 mm^2 incident beam and 0.025 x 10 mm^2 diffracted beam.

5.2.2. Measurement and recording requirements

Same requirements as described in section 5.1.2

5.3. Angle-dispersive X-ray diffraction

Transmission geometry is the simplest and most commonly used setup with monochromatic beam, but only provides a two-dimensional (2D) spatial resolution in a plane orthogonal to the beam direction (Reimers, 2008). Spatial depth resolved resolution within the bulk of the sample (3D) is accomplished using a conical slit cell (CSC). Alternatively, the spiral slit can also be available in some facilities. Its main drawback, when compared to the CSC, is that it does not allow the observation of complete rings, i.e. each spiral cuts a small fraction of the diffraction cone. Therefore, the application of the $\sin^2\psi$ method or depth resolved texture investigations are hindered.

Both techniques share some common standard procedures (assuming the use of 2D detectors) described in the following.

5.3.1. Preparation for measurements in ADXRD

a. Composition of the parts of the stage

The setup requires at least movements of the sample in x and z directions for the transmission geometry, and in x, y, and z for the CSC. This can be achieved with either an Eulerian cradle (and a z movement stage) or different motors assembled independently. For the latter, it is convenient to mount a rotation stage on top for aligning one of the sample's edges (if the sample exhibits a flat face) parallel to the beam, and finally rotating the sample during the measurement (e.g. for the strain in the third direction).

b. Detector positioning

The requirements differ depending on the technique:

- Transmission: the decision is based on the number of rings to analyse (typically only first order reflexion peaks are needed) and the phase lattice parameter.
- CSC: larger radii of the Debye-Scherrer rings are less prone to errors than small ones.

For using the full detector area, the beam should be approximatively at the centre of the detector (see Figure 39). As a rule of good practice, the effective sample-detector distance X can be calculated as follows in Eq. 16:

$$X £ 0.9´D = 0.9´\frac{P/2}{tg(2q)} \qquad \text{Eq. 16}$$

where D is the theoretical sample-detector distance, P is the minimum dimension of the detector array and q is the diffraction angle. A descriptive example might be the following for the transmission technique:

- Austenitic steel with a lattice parameter of 0.36 nm.
- $2D$ detector with an array of $2048´2048$ pixels, and a pixel size of $200´200$ μm², i.e. $\frac{P}{2} = 2048 * \frac{0.2}{2} = 204.8$ mm.
- Energy set to 87.1 keV ($l = 0.01423$ nm).

Assuming that only information from the first-order peaks is required, for an FCC lattice (331) is the crystallographic plane with the highest $h^2 + k^2 + l^2$ (h, k, l are the Miller indices), and its interplanar distance $d = 0.08259$ nm. By using Bragg's law as in Eq. 17:

$$l = 2dsinq \qquad \text{Eq. 17}$$

with l the wavelength, d the interplanar distance, and q with its common meaning, the $2q$ angle equals 9.888°. Substituting this term in Eq. 17 gives $D = 1175$ mm. This distance represents an upper limit. A good practice is to multiply it by ~ 0.9, which leads to $X \pounds 1058$ mm.

For the CSC a similar methodology applies, but with the aim to increase the selected radius (or radii) of the Debye-Scherrer ring as much as possible. It is worth remembering that the setup restricts the energies. A detailed subsection will address the energy selection for the CSC.
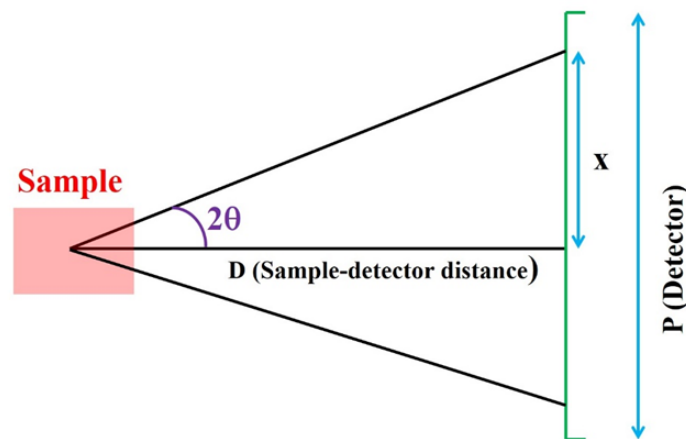
Figure 39 - Sketch showing different dimensions of the setup.

c. Optical laser

An optical laser is positioned before the slits that shape the beam. When correctly aligned, pointing in the direction of the beam, it is very useful for aligning:

- Beam stop
- CSC
- Sample

The instrumental setup before the slits usually remains unaltered or with minor modifications. Once the laser beam is aligned, it should be stable or undergo little modifications with time. In order not to block the beam, a good practice is to install it on a rail orthogonal to the beam to move it at convenience. The simplest procedure to align it is by scanning with the synchrotron beam and a photodiode a reference sample with a well-defined edge. After this operation, the laser beam can be aligned by pointing it to the edge of the sample.

d. Beam stop

The incoming beam is usually blocked by a beam stop in front of the detector to avoid damage (Fig. 40). Even when the sample diffracts the incoming beam, part of it is transmitted at high photon energy. The laser beam can be used to place it correctly. Its size has to be small enough to prevent partial blocking the Debye-Scherrer rings.
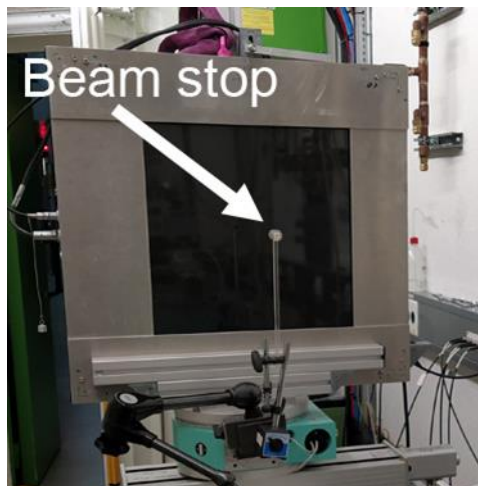
Figure 40 - Beam stop placed before a 2D detector.

e. Sample alignment using a photodiode

A photodiode is a passive transducer of photons into an electrical current. It serves to determine the edges (in x and/or z directions) of the sample much faster and more accurately than with the synchrotron beam and the detector. Its operation requires a permanent opening of the shutter. To prevent damage in the 2D detector, it is advisable to protect it with a steel or lead plate or similar during this process. It should be positioned with its centre coincident with the beam (using the laser), and, when possible, fixed to an element independent of the sample stage to prevent its displacement.

The placement of the photodiode depends on the technique:

- Full transmission: anywhere between the sample and the beam stop.
- CSC: between the sample and the CSC.

An alignment of the sample also requires the faces to be fully parallel to the beam as shown in Fig. 41 (otherwise, during the movement of the sample, the scanned lines may show some deviations from the theoretical lines, being relevant in the presence of large stress gradients). There are two options for this alignment:

- To install a camera above the sample, with a crosshair aligned in the beam direction.
- To use the sample rotation stage mentioned in a) together with the photodiode. A simple scan can easily determine the correct orientation of the sample.
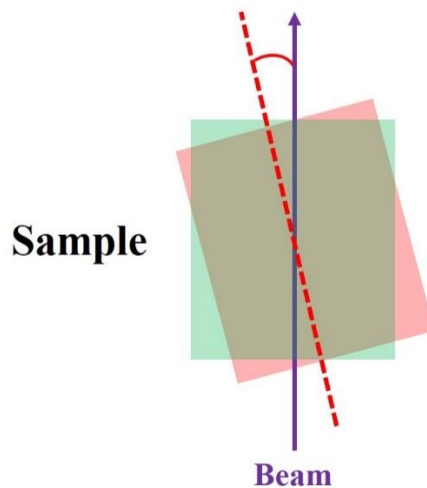
Figure 41 - Zenithal view sketch of a sample correctly aligned in the beam direction (green) and misaligned (red).

A final recommendation is a simple horizontal alignment using a level that allows observing a sample shift in z direction, when the sample is scanned either in x or in y direction (Figure 4242).
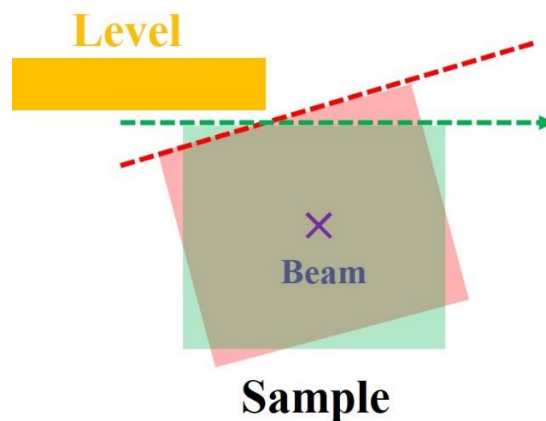
Figure 42 - Frontal view sketch of a sample with horizontal alignment (green) and misaligned (red).

f. Sample-detector distance and instrumental broadening calibration

LaB_6 and CeO_2 are frequently used as reference standards with a monochromatic beam to calibrate both sample-detector distance and instrumental peak profile. The powders are contained in capillaries/containers ranging from 1 mm up to 5 mm thickness. It is advisable to measure them at the beginning of the experiment for both the transmission geometry and conical slits to avoid forgetfulness later.

5.3.2. Transmission geometry (2D spatial resolution)

Only samples with a plane stress-state are suitable for this technique, i.e. simulations are required before performing the experiment in order to ensure the viability of the experiment. The acquired

Debye-Scherrer rings contain information integrated along the beam path without any resolution (provided uniquely by the sample thickness).

a. Energy selection

The energy has to be selected as function of different parameters:

- Sample thickness
- Material
- Flux

Changing the energy is usually done by the scientist responsible of the beamline.

b. Beam dimensions

The size of the gauge volume is defined by the incident beam size (in horizontal and vertical directions) and the sample thickness in the beam direction. The decision on the beam dimensions is be based on:

- Finite element modelling (FEM) simulations: it is not necessary to use a square beam section, but it can be varied in each direction so that the stress gradient affects as little as possible.
- Material microstructure: large grain sizes require larger slit sizes than refined microstructures.

c. Centre of the gauge volume for standard reference/sample positioning

To centre the gauge volume to be measured, different strategies have been developed.

- If there are permanent clamps to hold the sample, the position at which they join can be determined as the centre of the gauge volume.
- If not available, some marks should be made on the stage aligned with the centre of the LaB6 capillary/container to serve as a reference for positioning the sample.
- An optical camera with its centre placed at the centre of the LaB_6 capillary will automatize further alignments.

5.3.3. Conical slits (3D spatial resolution)

a. Advantages of the Eulerian cradle

Identical to the experiments with a white beam, an Eulerian cradle facilitates the correction of pseudo-strains with a double immersion scan. The main drawbacks for its use are linked to the focal distance of the CSC and the Eulerian cradle dimensions.

b. Ring and energy selection

The CSC typically possesses several conical slits with different radii. The decision which ring to use (once the crystallographic plane is selected) depends on several factors listed in the following and has to be a compromise between them.

- The energy required to get a good peak-intensity-to-background-ratio.
- Exposure time.
- Maximum energy available at the beamline.
- The optimal length of the gauge volume (the larger the radius of the CSC, the smaller the length), which is a function of the microstructure of the material and possible stress gradients (as for the transmission technique).
- Depending on the design of the CSC, it may be possible to track two or more crystallographic planes simultaneously (relevant for texture analysis), and consequently the energy should be adjusted so that the diffraction beam passes through these rings.

For example, for the measurement of the austenitic steel sample detailed above, if the ring radius is 13.1996 mm, and the crystallographic plane (311) is analysed, the energy required (with a focal distance of 100 mm) can be calculated as follows:

$$d_{311} = \frac{a}{\sqrt{h^2 + k^2 + l^2}} = \frac{0.36}{\sqrt{3^2 + 1^2 + 1^2}} = 0.10854 \text{ nm} \qquad \text{Eq. 18}$$

$$tg(2\theta) = \frac{Radius\ of\ the\ ring}{Focal\ distance} = \frac{13.1996 \text{ mm}}{100 \text{ mm}} \rightarrow 2\theta = 7.5193° \qquad \text{Eq. 19}$$

$$l = \frac{h \times c}{E} = 2'd'sinq \ \rightarrow E = \frac{h \times c}{2'd'sin\theta} \qquad \text{Eq. 20}$$

$$E = \frac{h \times c}{2 \times d \times sin\theta} = \frac{1.23985 \text{ keV nm}}{2 \times 0.10854 \text{ nm} \times \sin\left(\frac{7.5193°}{2}\right)} = 87.1 \text{ keV} \qquad \text{Eq. 21}$$

c. Beam size

The beam size typically ranges between $50 - 200 \, \mu m$. Below a beam size of $50 \, \mu m$, the depth resolution does not decrease further, because it is limited by the energy resolution given by the monochromator (Staron, 2014 (a)) (Staron, 2014 (b)). For further improvements of depth resolution, a reduction of the energy bandwidth is needed.

As for the transmission technique, prior knowledge of the stress gradients and the material microstructure is necessary to define the beam dimensions.

d. Small hexapod and preliminary alignment of the CSC

The CSC is mounted on a small hexapod (see Fig. 43) with movements independent of the sample stage. An initial alignment of the position of the CSC can be done using the alignment laser. A simple and effective method for pre-alignment of the orientation of the CSC is to stick a small mirror outside the rings and rotate the hexapod until the optical laser reflects into itself. With subsequent rotations around the x, y, and z axes (see Fig. 44), the diffracted signal must coincide with the laser beam on the

slits. Once the CSC is correctly oriented, it is only necessary to move it until the laser beam roughly coincides with the centre of the CSC. This simple methodology ensures a good starting position for a subsequent further fine alignment with the beam.

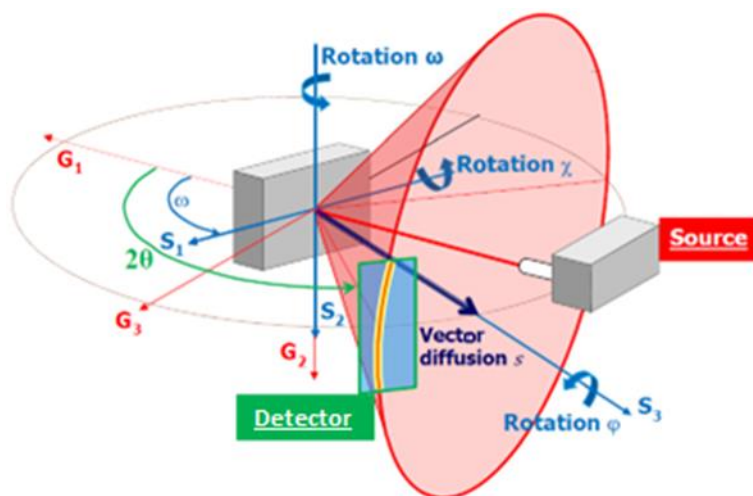*Figure 43 - View of the mini-hexapod together with the CSC attached to it.*

Figure 44 - 3D representation, with the definition of the ω, χ and φ angle.

e. Fine alignment of the CSC

The CSC alignment requires high precision to ensure that the Debye-Scherrer cones pass exactly through the rings (otherwise they can be partially blocked). In the first step, the centre of the CSC has to be placed in the centre of the beam by shifting the CSC horizontally (x) and vertically (z). In a second step and to avoid that the local spot leaves the beam, the rotation axes are placed in the focal point. This is easily done with the hexapod setting the pivot point.

The pivot point should be at the centre of the CSC (rather than at the centre of the hexapod). A ruler is enough to measure the distances in z and y between the centres of the hexapod and the CSC.

If raw powders of the alloy under investigation (with identical chemical and heat-treated conditions) were available, they should fill a container with a typical thickness of $0,5 - 1$ mm. Since in most cases this is not possible, a thin plate $0,5 - 1$ mm thick machined out with electrical discharge machining (EDM) from the sample (if possible) is also a suitable option, if the microstructure is fine. But even with a refined microstructure, the presence of local microtextures results in local intensity variations affecting the intensity. Coarse grains do not show continuous Debye-Scherrer rings, and the adjustment is not precise.

There is no standard method for this task. The goal is that all four quarters of the Debye-Scherrer ring become homogeneous and with similar intensities. It is necessary to vary rotation angles (around x, y, and z) and x and z positions, until this objective is achieved.

f. Gauge volume length and centre determination

With the CSC correctly aligned, it only remains to scan in the beam direction y the powders/thin plate to determine the effective length of the gauge volume. By analysing the integrated intensity, the effective length of the gauge volume is defined as the FWHM of the peak (Staron, 2014 (a)) (Staron, 2014 (b)). A Gaussian curve is typically used for the fitting. As example, a 1 mm thick austenitic steel plate is scanned in y direction to find the centre and gauge length magnitudes (Fig. 45).
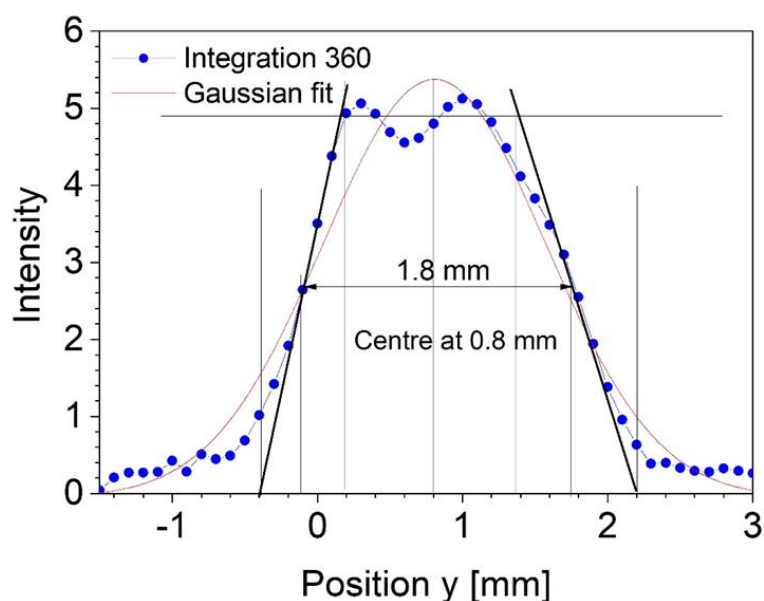

Figure 45 - Integrated intensity variation of the scanned thin austenitic plate. The line is fitted with a Gaussian curve.

The focal point in this example is at $y = 0.8$ mm of the stage coordinates, i.e. 100 mm from the CSC. It can be cross-checked with a ruler and, if available, a camera or a theodolite can be used to spatially fix this point as a reference for further measurements.

g. Sample positioning in y direction

As commented above, a ruler, a camera or a theodolite are valid to align a sample in y direction. A ruler can be precise enough as a consequence of the elongate gauge volume and little contributions from the sides.

h. Sample measurement

For the sample measurement, the same procedure as indicated for the transmission technique is followed. The main difference lies in the exposure time, since it is usually much higher than for the transmission case. Acquisition times of even minutes can be normal for thick samples.

5.4. Neutron diffraction

5.4.1. Preparation for measurements

Before starting a measurement, it is necessary to calibrate the instrument and check or carry out the alignment of the instrument. Based on the report D2.1 from the project Brightness 2, the calibration and alignment of a neutron instrument are detailed in the following sections (Brightness, 2020).

a. Instrument calibration

Calibration measurements are performed to ensure the accuracy of the absolute position of the Bragg's peaks in the wavelength or Time-Of-Flight (TOF) spectrum. Elemental powders, typically silicon, ceria, or alumina are used, since they diffract neutrons well, have known d-spacing and non-overlapping diffraction peaks, exhibit a fine grain size, and are free of macrostresses. The angular (on a monochromatic instrument) or the temporal (on a TOF instrument) positions of the Bragg's peaks are then compared against the tabulated data, and the instrument is calibrated accordingly.

b. Instrument alignment

Instrument alignment involves adjusting the beam optics components (slits and collimators) to ensure that the reference point, i.e., the centroid of the gauge volume, coincides with the centre of the ω-rotation axis to allow changing the measurement direction by rotating the sample without any need of re-alignment. Generally, an instrument alignment is performed every time there is a configuration change in the optical path, e.g., changing from slit to radial collimator setup, and prior to sample characterisation. While there are slight variations of the procedures among instruments, the underlying principles are the same. The main steps of the instrument alignment techniques are given below.

1.   Find the centre of the ω-rotation axis.

2.   Adjust the sample alignment system to the centre of ω-rotation axis.

3.   Align the beam apertures optical axes.

5.4.2. Measurement and recording requirements

Stress and strain in most engineering components usually have directional and positional dependence, which requires measuring strain at a number of locations, i.e., strain mapping. This is achieved by translating and rotating the sample stage to desired positions. Most neutron diffraction investigations involve a general three-dimensional stress state that requires measurements along the principal (maximum) strain directions in three mutually orthogonal directions. After positioning the sample for a specific measurement, the diffracted intensity is recorded for a specified measurement time or number of counts. The general procedure for residual stress analysis at a single measurement point is described in the following.

a. Mount and align the sample for the measurement of strain along the first direction

Secure the sample on the sample stage (directly, via Eulerian cradle, or another sample environment). Using the sample positioner system (xyz-translation stage or hexapod) align the sample so that the measurement point, indicated by the green circle in Fig. 46(A), is accurately positioned at the reference point, Fig. 46(B), coinciding with the centre of the ω-rotation axis shown by the red cross in Fig. 46(B). The sample alignment is carried out with the help of the sample alignment system, which can be either mechanical or optical. Finally, the ω-angle and angular detector positions are adjusted according to the strain direction for the desired reflection. Measure the diffracted signal against the specified measurement time.

b. Measurement of strain along the second direction

For instruments with a single position-sensitive detector (PSD), the measurement in the second horizontal strain direction is performed by rotating the sample stage along the ω-axis, Fig. 46(C) by 90°, when in principal direction. Since the reference point coincides with the centre of ω-rotation, no additional sample alignment is needed. While not applicable for instruments within the EASI-STRESS project, there are also instruments with two detector banks (e.g. ENGINE-X at ISIS). There, two orthogonal strain components are acquired simultaneously in one measurement, Fig. 46(B).

c. Measurement of strain along the third direction

For most instrument configurations (xyz-stage and hexapod), the measurement in the third strain direction is achieved by removing and manually rotating the sample to have the desired direction along the scattering vector. This requires that the sample is re-mounted and re-aligned to enable a measurement at the same position of the previous measurements, Fig. 46(D). Note that by using an Eulerian cradle or a robotic arm, this step can be performed without sample remounting.

d. Measurement of another reflection and/or strain component

For special cases, such as composite materials and/or complex stress states, measurements of strains for more than 3 directions and/or for more than one hkl reflection is required and therefore other $2\theta_{det}$ and/or other angular orientations are necessary Fig. 46(E).
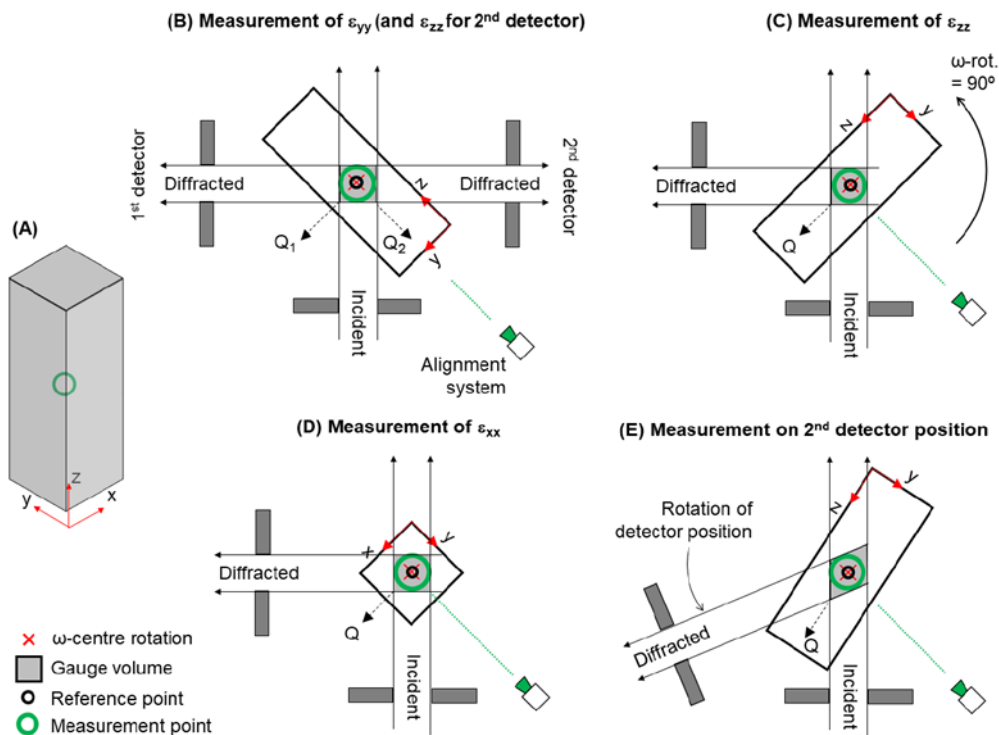

Figure 46 - Illustration of strain measurement steps at a neutron strain scanner with two detectors: (A) The sample and its coordinate system, with a desired measurement point indicated by the green circle; (B) Alignment of the measurement point to the instrument reference position and the measurement of the ε_{yy} with the first detector and the ε_{zz} with the second detector; (C) Measurement of the ε_{zz} by rotating the sample along ω by 90°; (D) Measurement of the ε_{xx} after removing and manually rotating the sample about the y-axis of the sample by 90° followed by re-mounting and re-alignment; (E) Measurement of another hkl reflection by changing the detector position.

5.5. X-ray laboratory diffraction

The XRD measurement method is based on the strain quantification. Only two angles are useful to define the direction of the measured strain: Ψ and Φ angles illustrated just below in Fig. 47.
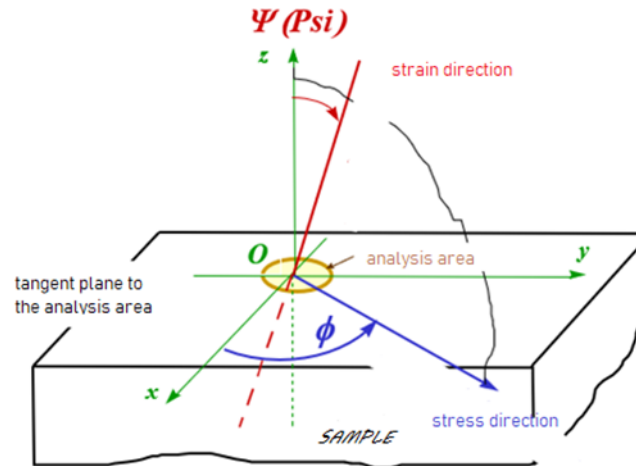
Figure 47 - Relation between strain and Bragg's angle.

The Bragg's law application can also be represented by focusing on the source and detector position. 1D or 3D spatial representation are given in Fig. 44.

The definition and the impact of all the different axis on the measurement is listed below:

- Scan in the S_1 direction gives the ε_{11} strain value.
- Scan in the S_2 direction gives the ε_{22} strain value.
- Scan in the S_3 direction is impossible, that's why measuring the full tensor is quite complicated by X-Ray diffraction.
- 2θ diffraction angle applied to the detector system.
- ω and χ are directly impacting the sample orientation and consequently the peak localization.

The principle is then to have 2θ scans of the sample surface through S_1 and S_2 vectors and with different Ψ angles (or sample orientations with ω rotations e.g.).

References

Als-Nielsen, D. M. (2011). *Elements of modern X-ray physics.* John Wiley & Sons.

Apel. (2018). Residual stress analysis of energy-dispersive diffraction data using a two-detector setup: Part I — Theoretical concept. *Nuclear Instruments and Methods in Physics Research, Section A: Accelerators, Spectrometers, Detectors and Associated Equipment 877*, 24-33.

Apel, M. K. (2014). Rietveld-based energy-dispersive residual stress evaluation: analysis of complex stress fields σ_{ij} (z). *Journal of Applied Crystallography, 47*, 511-526.

Brightness. (2020). Deliverable Report D.2.1 Preliminary report on engineering: Calibration protocol for all strain scanning instruments and definition of criteria for the Neutron Quality Label.

Dejoie. (2018). Combining a nine-crystal multi-analyser stage with a two-dimensional detector for high-resolution powder X-ray diffraction. *Journal of Applied Crystallography, 51*.

Denks, C. G. (2007). Enhancement of energy dispersive residual stress analysis by consideration of detector electronic effects. *Nuclear Instruments and Methods in Physuscs Research B, 262*, 87-94.

EN15305:2009, S. (2009). *EN15305 (2009) - Test Methods for residual stress analysis by X-ray diffraction.*

Felcher, G. (1989). Industrial applications of neutron diffraction. *Hyperfine Interactions, 45(1)*, 127-142. Retrieved from https://doi.org/10.1007/BF02405876

Fitch, A. (2019). Synchrotron radiation and powder diffraction, International Tables for Crystallography, Vol H, Chapter 2.2.

François, M. (2008). Unified description for the geometry of X-ray stress analysis: proposal for a consistent approach. *Journal of Applied Crystallography, 41*, 44-45.

Gelfi, E. B. (2004). X-ray diffraction Debye Ring Analysis for STress measurement (DRAST): a new method to evaluate residual stresses. *M. Gelfi, E. Bontempi, R. Roberti, L. E. Depero, X-ray diffraction Debye Ring AnalysActa Materialia, 52*, 583-589.

He, B. B. (2009). *Two-dimensional X-ray diffraction.* Jhon Wiley & Sons.

Honkimaki, P. S. (2007). Energy-dispersive diffraction with synchrotron radiation and a germanium detector. *Journal of Synchrotron Radiation, 14*, 331-338.

ID22. (n.d.). *https://www.esrf.fr/id22/technical-description.*

Lienert, R. M. (2000). High spatial resolution strain measurements within bulk materials by slit imaging. *Materials Research Society Symposium Proceedings*, 241-246.

Martins. (2003). Depth resolved strain and phase mapping of dissimilar friction stir welds using high energy synchrotron radiation. *Textures and Microstructures, 35, No 3/4*, 145-152.

Martins. (2005). Determination of the radial crystallite microstrain distribution within an AlMg3 torsion sample using monochromatic synchrotron radiation. *Materials Science & Engineering A*, 278-287.

Mobilio, F. B. (2015). *Synchrotron Radiation Basics, Methods and Applications.* Springer.

Oed, A. (2004). Detectors for thermal neutrons. Nuclear Instruments and Methods. *Physics Research Section A: Accelerators, Spectrometers, Detectors and Associated Equipment, 525 (1)*, 62-68.

P07(a). (n.d.). *https://photon-science.desy.de/facilities/petra_iii/beamlines/p07_high_energy_materials_science/optics/index_eng.html.*

P07(b). (n.d.). *https://photon-science.desy.de/sites/site_photonscience/content/e58/e176720/e177229/e178413/e178444/e178445/infoboxContent178446/Heavyloadhexapod_eng.pdf.*

P07(c). (n.d.). *https://photon-science.desy.de/facilities/petra_iii/beamlines/p07_high_energy_materials_science/detectors/index_eng.html.*

P61A(a). (n.d.). *https://photon-science.desy.de/facilities/petra_iii/beamlines/p61_high_energy_wiggler_beamline_lvp/p61a_white_beam_engineering_materials_science_hzg/index_eng.html.*

P61A(b). (n.d.). *https://photon-science.desy.de/facilities/petra_iii/beamlines/p61_high_energy_wiggler_beamline_lvp/p61a_white_beam_engineering_materials_science_hzg/index_eng.html.*

P61A(c). (n.d.). *https://photon-science.desy.de/facilities/petra_iii/beamlines/p61_high_energy_wiggler_beamline_lvp/index_eng.html.*

Petry, W. (2015). Neutrons for industry. (p. 1001). EPJ Web of Conferences, 104. Retrieved from https://doi.org/10.1051/epjconf/201510401001

Pirling. (2006). *Materials Science and Engineering A 437*, 139-144.

Reimers, A. P. (2008). *Neutrons and Synchrotron Radiation in Engineering Materials Science.* WILEY-VCH.

Rowles, M. R. (2011). On the calculation of the gauge volume size for energy-dispersive X-ray diffraction. *Journal of Synchrotron Radiation, 18*, 938-941.

Staron. (2014 (a)). Depth-resolved residual stress analysis with conical slits for high energy X-rays. *Mater. Sci. Forum 772*, 3-7.

Staron. (2014 (b)). Depth-resolved residual stress analysis with high-energy synchrotron X-rays using a conical slit cell. *P. Staron, T. Fischer, J. Keckes, S. Schratter, T. Hatzenbichler, N. Schell, M. Müller, A. Schreyer, Depth-resolMater. Sci. Forum 768-769*, 72-75.

Suzuki, M. (2014). Recent trends in industrial applications. *Synchrotron Radiation News 27(3)*, 2. Retrieved from https://doi.org/10.1080/08940886.2014.908696